Dynamic Modeling and Stability Study of Microturbine with PMSG in Distributed Generation

by:

Md. Ishtiak Ahmed Tuham (112411)

Syed Raihan Hossain (112421)

Md. Abrar Amin (112423)

BACHELOR OF SCIENCE IN ELECRTICAL AND ELECTRONIC ENGINEERING

ISLAMIC UNIVERSITY OF TECHNOLOGY (IUT)

A Subsidiary Organ of Organization of Islamic Cooperation (OIC)
Dhaka, Bangladesh.
November, 2015

Dynamic Modeling and Stability Study of Microturbine with PMSG in Distributed Generation

by:

Md. Ishtiak Ahmed Tuham (112411)

Syed Raihan Hossain (112421)

Md. Abrar Amin (112423)

A Dissertation Submitted in partial fulfillment of the requirement for the award of the degree of

Bachelor of Science in Electrical and Electronic Engineering

Academic Year: 2014-15

ISLAMIC UNIVERSITY OF TECHNOLOGY (IUT)

A Subsidiary Organ of Organization of Islamic Cooperation (OIC)
Dhaka, Bangladesh.
November, 2015

Declaration of Authorship

We, Md. Ishtiak Ahmed Tuham (112411), Syed Raihan Hossain (112421) and Md. Abrar Amin (112423), declare that this thesis titled, 'Dynamic Modeling and Stability Analysis of Microturbine with PMSG in Distributed Generation' and the works presented in it are our own. We confirm that:

- This work has been done for the partial fulfillment of the Bachelor of Science in Electrical and Electronic Engineering degree at this university.
- Any part of this thesis has not been submitted anywhere else for obtaining any degree.
- Where we have consulted the published work of others, we have always clearly attributed the sources.

Submitted by:

_____

Md. Ishtiak Ahmed Tuham (112411)

_____

Syed Raihan Hossain (112421)

_____

Md. Abrar Amin (112423)

Dynamic Modeling and Stability Analysis of Microturbine with PMSG in Distributed Generation

Approved By:

Ashik Ahmed

Thesis Supervisor,

Assistant Professor

Department of Electrical and Electronic Engineering,

Islamic University of Technology.

Prof. Dr. Md. Shahid Ullah

Head of the Department,

Department of Electrical and Electronic Engineering,

Islamic University of Technology.

Abstract

Distributed generation (DG) is attracting more attention recently as an alternative to large centralized generation plants, driven by the rapidly evolving deregulation environments. Among the different sources of DG, the microturbine generation (MTG) system has a good record of improving the system stability, reliability and power quality. This thesis is aimed on the dynamic performance enhancement of a permanent-magnet synchronous generator (PMSG) based MTG system connected to a distribution system through an AC-to-DC converter and a DC-to-AC inverter. The switching parameters for the converter and inverter are controlled by PI controllers and the controller parameters are selected using Genetic Algorithm. The overall dynamic model is presented in the synchronously rotating reference frame *dq*-axis. Simulations of the studied MTG are carried out using MATLAB.

Acknowledgements

First and foremost, we offer gratitude to the Almighty Allah (SWT) for giving us the capability to do this work with good health.

We are grateful to our research supervisor, Ashik Ahmed, for the support and guidance throughout our research at Islamic University of Technology (IUT) since January, 2015. He created a research environment for which we were able to explore many ideas without constraint. We have gained a wealth of knowledge and experience in science and engineering through his direction that is beyond value to our future endeavor. For these things, we give many thanks to him.

We would like to thank all the faculty members of the department of EEE, IUT for their inspiration and help.

And last but not the least we are thankful to our family, friends and well-wishers for their support and inspiration. Without them it would never have been possible for us to make it this far.

Contents

List of Figures

List of Tables

Abbreviations

DG	**D**istributed **G**eneration
PMSG	**P**ermanent **M**agnet **S**ynchronous **G**enerator
MTG	**M**icroturbine **G**enerator

Dedicated to our parents...

Chapter 1

Introduction

1.1 Distributed generation

Distributed generation is an approach that employs small-scale technologies to produce electricity close to the end users of power. DG technologies often consist of modular (and sometimes renewable-energy) generators, and they offer a number of potential benefits. In many cases, distributed generators can provide lower-cost electricity and higher power reliability and security with fewer environmental consequences than can traditional power generators.

In contrast to the use of a few large-scale generating stations located far from load centers--the approach used in the traditional electric power paradigm--DG systems employ numerous, but small plants and can provide power onsite with little reliance on the distribution and transmission grid. DG technologies yield power in capacities that range from a fraction of a kilowatt [kW] to about 100 megawatts [MW]. Utility-scale generation units generate power in capacities that often reach beyond 1,000 MW.

The current model for electricity generation and distribution in the United States is dominated by centralized power plants. The power at these plants is typically combustion (coal, oil, and natural) or nuclear generated. Centralized power models, like this, require distribution from the center to outlying consumers. Current substations can be anywhere

from 10s to 100s of miles away from the actual users of the power generated. This requires transmission across the distance.

This system of centralized power plants has many disadvantages. In addition to the transmission distance issues, these systems contribute to greenhouse gas emission, the production of nuclear waste, inefficiencies and power loss over the lengthy transmission lines, environmental distribution where the power lines are constructed, and security related issues.

Many of these issues can be mediated through distributed energies. By locating, the source near or at the end-user location the transmission line issues are rendered obsolete. Distributed generation (DG) is often produced by small modular energy conversion units like solar panels. As has been demonstrated by solar panel use in the United States, these units can be stand-alone or integrated into the existing energy grid. Frequently, consumers who have installed solar panels will contribute more to the grid than they take out resulting in a win-win situation for both the power grid and the end-user.

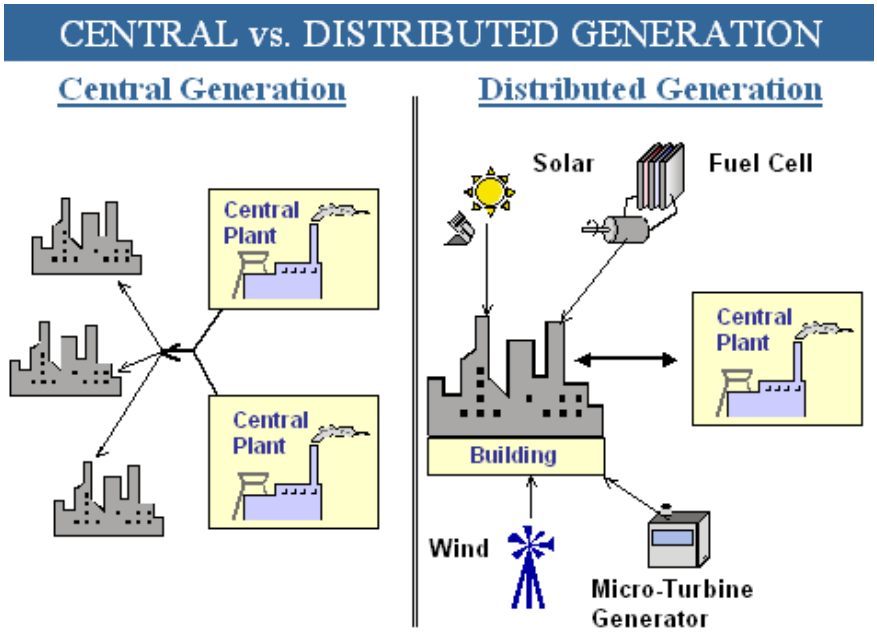

Fig.1.1: Distributed Generations

Some examples of DG technologies:

There are various DG sources using which we can generate electricity. These are microturbine generation, solar energy, wind power generation, fuel cell etc.

Fig.1.2: Wind turbine

Fig.1.3: Microturbine generators

1.2 Microturbine Generators

Microturbine Generators are a relatively new distributed generation technology being used for stationary energy generation applications. They are a type of combustion turbine that produces both heat and electricity on a relatively small scale.

1.2.1 Typical Microturbine Construction

Microturbines are a simple form of gas turbine, usually featuring a radial compressor and turbine rotors and often using just one stage of each. They typically recover exhaust energy to preheat compressed inlet air, thereby increasing electrical efficiency compared with a simple-cycle machine. The air-to-air heat exchanger is termed a “recuperator” and the entire system is typically called a recuperated cycle.

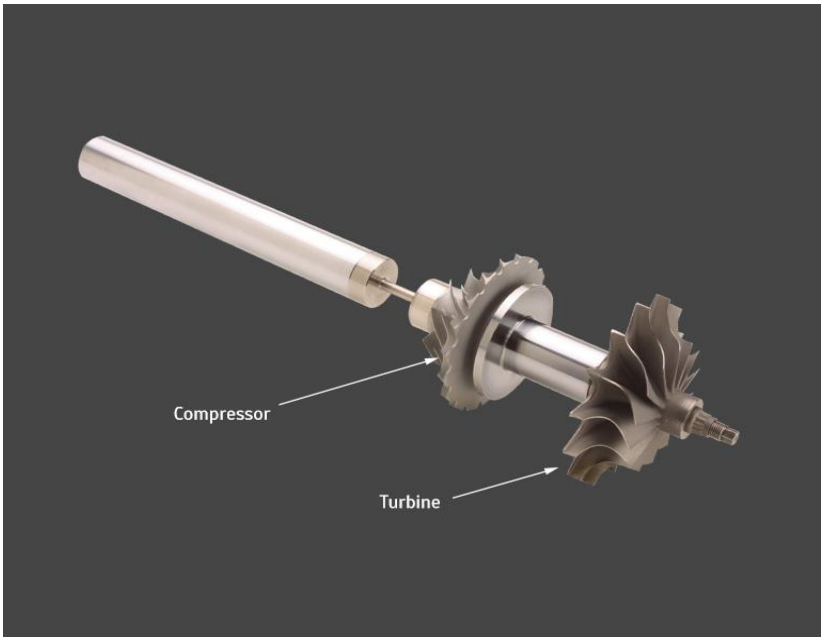

Fig.1.4: Microturbine

Fig. 1.4 shows a 50kW high speed alternator rotor mounted with the compressor & turbine. Its length is only 25cm.

So basically the important components of a microturbine generator system is:

1. Compressor
2. Combustor
3. Turbine
4. Generator

1.2.2 Advantages

<u>Aesthetics</u>:

- Improves sightlines and views with off-the-grid systems, which eliminate the need for overhead power lines

Cost-Effective:

- Enables cost savings by reducing the peak demand at a facility, therefore lowering demand charges

Functional:

- Provides better power reliability and quality, especially for those in areas where brownouts, surges, etc. are common or utility power is less dependable
- Provides power to remote applications where traditional transmission and distribution lines are not an option such as construction sites and offshore facilities
- Can be an alternative to diesel generators for on-site power for mission critical functions (e.g., communications centers)
- Possesses combined heat and power capabilities
- Reduces upstream overload of transmission lines
- Optimizes utilization of existing grid assets—including potential to free up transmission assets for increased wheeling capacity
- Improves grid reliability
- Facilitates faster permitting than transmission line upgrades
- Can be located on sites with space limitations for the production of power

Productive:

- Provides high-quality power for sensitive applications
- Responds faster to new power demands—as capacity additions can be made more quickly
- Facilitates less capital tied up in unproductive assets—as the modular nature of microturbines means capacity additions and reductions can be made in small

increments, closely matched with demand, instead of constructing central power plants sized to meet estimated future (rather than current) demand

- Produces less noise than reciprocating engines

Secure/Safe:

- Strengthens energy security
- Stand-by power provides quick recovery after an event

Sustainable:

- Produces the lowest emission of any non-catalyzed fossil fuel combustion system
- Has a small footprint, minimizing site disturbance
- Reduces or defers infrastructure (line and substation) upgrades
- For recuperated microturbine, possesses higher energy conversion efficiencies than central generation
- Enables more effective energy and load management

1.2.3 Disadvantages

- Loss of power output and efficiency with higher ambient temperatures and elevation.
- Low fuel to electricity efficiencies.

1.2.4 Economics of Microturbines

Microturbine capital costs range from $700-$1,100/kW. These costs include all hardware, associated manuals, software, and initial training. Adding heat recovery increases the cost

by $75-$350/kW. Installation costs vary significantly by location but generally add 30-50% to the total installed cost.

Microturbine manufacturers are targeting a future cost below $650/kW. This appears to be feasible if the market expands and sales volumes increase.

With fewer moving parts, microturbine vendors hope the units can provide higher reliability than conventional reciprocating generating technologies. Manufacturers expect that initial units will require more unexpected visits, but as the products mature, a once-a-year maintenance schedule should suffice. Most manufacturers are targeting maintenance intervals of 5,000-8,000 hours.

Maintenance costs for microturbine units are still based on forecasts with minimal real-life situations. Estimates range from $0.005-$0.016 per kWh, which would be comparable to that for small reciprocating engine systems.

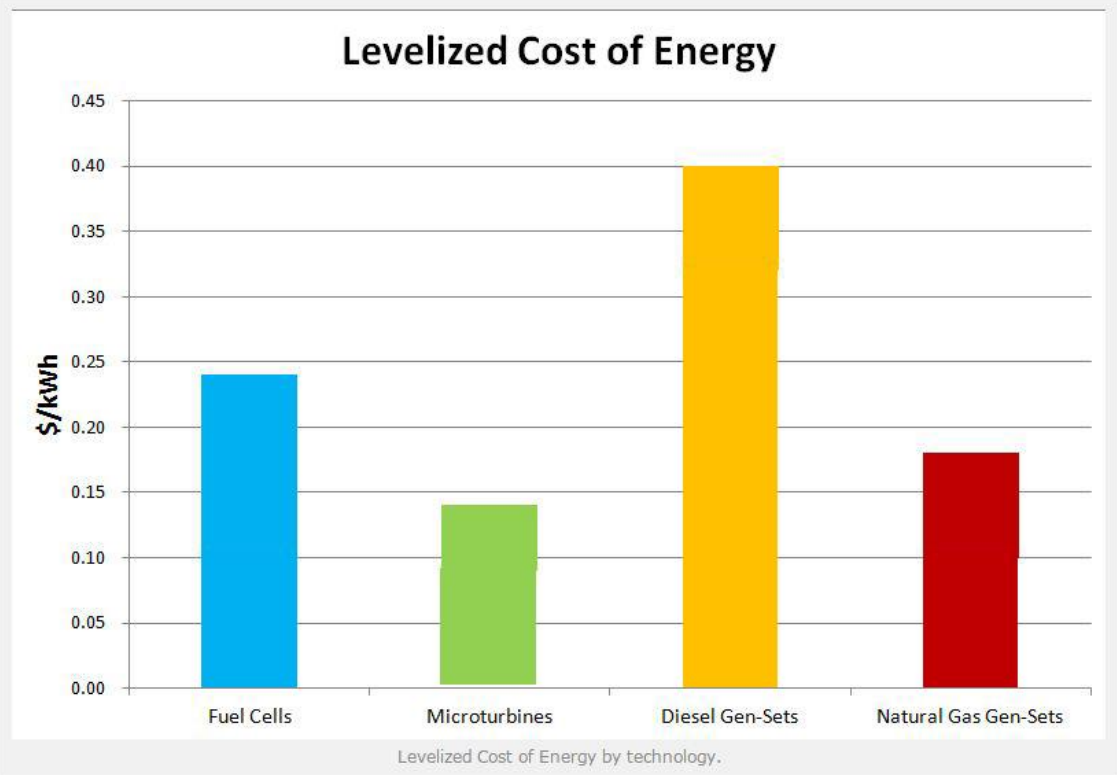

Fig.1.5: cost comparison of different DG technologies

1.3 Literature Review

A microturbine generation (MTG) system comprises of a microturbine driving an electrical generator. The following paragraphs give a brief summary on the earlier work done on the microturbine part of the MTG system as well as a brief review of its electrical generator part. Microturbines are small high-speed versions of conventional heavy-duty gas turbines. Hence the dynamic model of a conventional gas turbine, with relatively small thermodynamic constants, can be adopted to study the impacts of a microturbine on the overall system.

Rowen [1] was among the first ones who presented a model of a heavy-duty gas turbine suitable for use in dynamic power studies and in analyses of connected equipment. The author gave a mathematical model of a single-shaft gas turbine in terms of p.u. values. The control systems of the given model include speed control, acceleration control, and fuel system. Also, the developed model is suitable for both isolated and parallel operation.

Hannett and Afzal Khan [2], in continuation to Rowen's work, validated the gas turbine model by comparing its dynamic performance with that of an operating gas turbine generation system. The authors conclude that the model proposed by Rowen is adequate for the representation of a gas turbine.

In [3], the authors used the validated model of the gas turbine [2] to simulate the response of a combined cycle plant. Their system comprises of a gas turbine model and a steam turbine model which uses the waste heat from the gas turbine through a heat recovery system. This simulated (combined cycle) model can be used for system dynamic performance studies.

In an extension to this work, Jurado et al [4] studied the influence of microturbines on distribution networks stability. They also examined the transient and voltage stability of the system. The authors conclude that the microturbines, acting as distributed resources, are capable of providing effective load following service in a distribution system.

In [5] the authors utilize the proposed model of the microturbine to develop a control system with an adaptive controller for a fuel cell-microturbine hybrid power plant. The developed adaptive controller has the ability to stabilize the system for different

disturbances affecting the plant like load power variation or a change in the plant model parameters such as gas composition. Continuing their work in [6], the authors used auto-regression with exogenous signal (ARX) identification algorithm to arrive at the transfer-function of a microturbine model. These transfer-functions have the same dynamic response as the original dynamic model of the microturbine, with the added advantage of significant reduction in the model order.

Amer Al-Hinai and Ali Feliachi [7] presented a complete model of the MTG system, used as a distributed generator, by making use of the microturbine model discussed in the earlier paragraphs. It includes the power electronic interfacing and is suitable for transient analysis as well as simulation of unbalanced three-phase power system. This paper also presents the simulation results obtained in MATLAB/Simulink. The electric generator used in a modern MTG system is usually a permanent magnet synchronous generator (PMSG).

In [8] the authors introduced the long term dynamics model for stationary gas turbines, including the turbo generator, with especial attention for use in combined gas and steam (CGS) power plants. The gas turbine model is devoted to large rated power gas turbines, whose fluid mechanical time response is much larger than that for the fluid gas flow in its three compartments: compressor, combustion chamber and turbine.

Using this model in [9], a thermodynamic based micro-turbine model supplemented with experimental data & validated calculations is introduced. The data was extracted from a study on the 60 kW Capstone C60 Microturbine.

Nikkhajoei and Iravani [10] investigated the use of an AC–AC matrix converter, as an alternative to AC–DC–AC converter system, to interface a high-speed micro-turbine generator (MTG) to a utility grid as a distributed generation unit. They presented a new switching strategy and a control mechanism for the converter. The dynamic behavior of a micro-turbine generation system, including the dynamic models of the micro-turbine (thermodynamics), generator, matrix converter, converter control and micro-turbine control was studied based on time-domain simulations in the PSCAD/EMTDC environment.

In [11], Li Wang presented the analyzed results of a permanent-magnet synchronous generator-based microturbine generator (MTG) system connected to a distribution system through an AC-to-DC converter and a DC-to-AC inverter. The employed mathematical model based on a *dq*-axis reference frame is derived to establish the complete dynamic equations of the studied MTG system for simulating the characteristics of the MTG under various operating conditions.

Gaonkar and Patel [12] investigated the ability of microturbine units in distribution systems, their efficient modeling is required. This paper presents a dynamic model of a micro- turbine generator system. The model is developed in the MATLAB/Simulink and implemented in SimPowerSystems library.

Gaonkar and Nayak [13] presented modeling and performance analysis of MTG system in grid connected and islanding modes of operation. The model developed in this work includes the individual components of prime mover like, compressor, heat exchanger, burner and turbine. The MTG system uses a DC link voltage to control the microturbine output power by fuel and air flow control methodology. The DC link power is delivered to the load through a voltage source inverter (VSI) with pulse width modulation (PWM) technique. The model of MTG system has been implemented using Matlab/Simulink environment and its simulation result shows the load following performance of MTG system for various loads.

1.4 Thesis Objective

The main objective of this thesis is to develop a dynamic model of a grid-connected MTG system through power conditioning system and study and analyze the stability of the overall system. In detail:

- To develop a thermo-dynamic model of single-shaft, non-recuperated Microturbine, suitable for stability analysis in both standalone and grid connected mode.

- To use the dynamic model of Permanent Magnet Synchronous Generator (PMSG) on *dq*-axis reference frame to eliminate the complexity in grid connected analysis.
- To develop a dynamic model of the AC-to-DC converter and DC-to-AC inverter appropriate for *dq*-axis reference which is very much essential to connect the PMSG to the grid. To control the switching parameters by PI controllers and select the PI controller parameters by a highly efficient optimization tool called the Genetic Algorithm.

1.5 Thesis Organization

- In chapter 2, basic theory on microturbine, types and thermo-dynamic model have been described.
- Properties of permanent magnet, their properties, types, materials, making procedure are described in chapter 3. The dynamic model of Permanent Magnet Synchronous Generator is also presented in chapter 3.
- Chapter 4 contains the dynamic models of AC-to-DC converter and DC-to-AC inverter, along with their switching mechanisms and parameters are given.
- Basic theory on Genetic Algorithm (GA), mechanism, flow chart and the optimization of the PI controller parameters using GA have been shown in chapter 5.
- In chapter 6, the stability analysis and the results of simulations done in MATLAB, are presented.
- Chapter 7 contains the conclusion of the thesis, where the brief summary of the results is given. Also the extension of this work is described at the end of this chapter.

Chapter 2

Microturbine

2.1 Introduction

Microturbines are new form of small gas turbine, usually featuring a radial compressor and turbine rotors and often using just one stage of each. They typically recover exhaust energy to preheat compressed inlet air, thereby increasing electrical efficiency compared with a simple-cycle machine. The air-to-air heat exchanger is termed a "recuperator," and the entire system is typically called a recuperated cycle.

2.2 Types of Microturbine

Microturbine generators can also be divided into two general classes:

- *Non-recuperated microturbines*—In a simple cycle, or non-recuperated, turbine, compressed air is mixed with fuel and burned under constant pressure conditions. The resulting hot gas is allowed to expand through a turbine to perform work. Simple cycle microturbines have lower efficiencies at around 15%, but also lower capital costs, higher reliability, and more heat available for cogeneration applications than recuperated units.

- *Recuperated microturbines*—Recuperated units use a sheet-metal heat exchanger that recovers some of the heat from an exhaust stream and transfers it to the incoming air stream, boosting the temperature of the air stream supplied to the combustor. Further exhaust heat recovery can be used in a cogeneration configuration. The figures below illustrate a recuperated microturbine system. The fuel-energy-to-electrical-conversion efficiencies are in the range of 20 to 30%. In addition, recuperated units can produce 30 to 40% fuel savings from preheating.

2.3 Working Principle

The basic components of a microturbine generation system are: compressor, turbine, recuperator, high-speed generator and power electronics interfacing. In the following paragraphs a brief description of each component is given, followed by a detailed modeling of microturbine and high-speed generator.

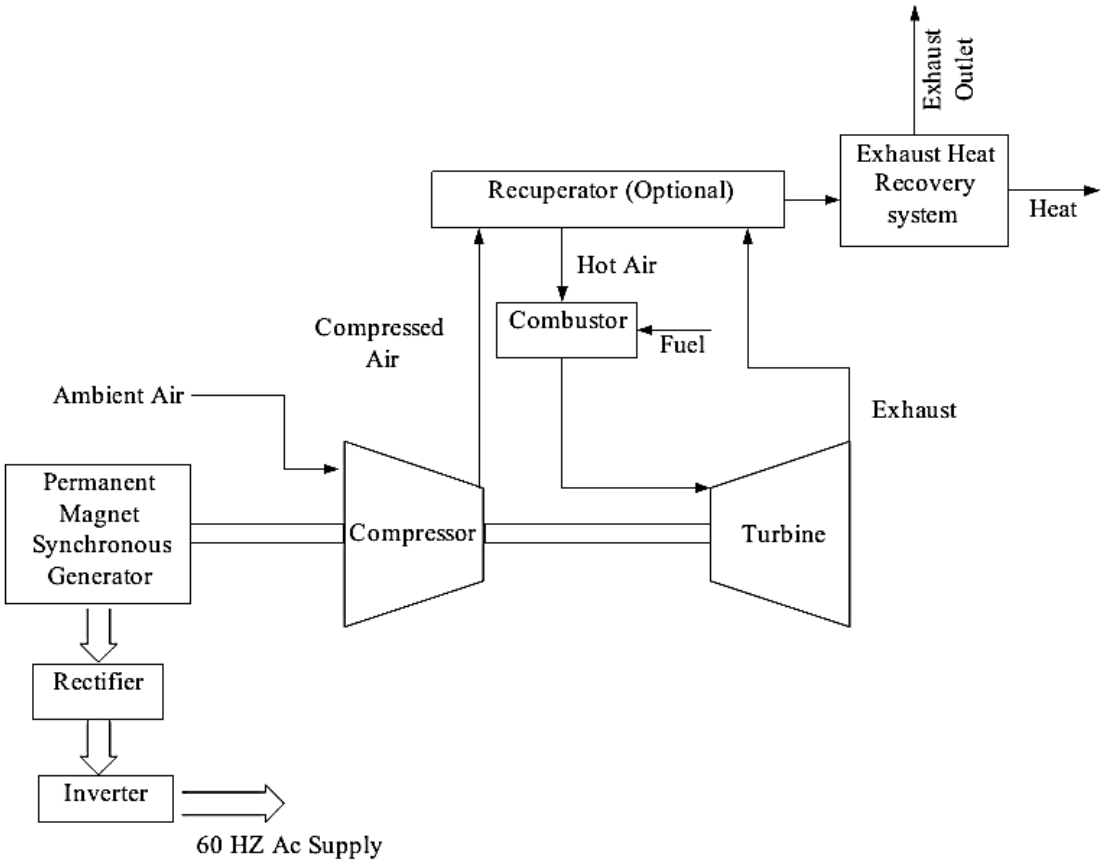

Fig. 2.1: Microturbine based CHP system (Single-Shaft Design)

Fig. 2.1 below shows the schematic diagram of a single-shaft microturbine based generation system.

Microturbines, like large gas turbines, operate based on the thermodynamic cycle known as the Brayton cycle [14]. In this cycle, the inlet air is compressed in a radial (or centrifugal) compressor. The compressed air is mixed with fuel in the combustor and burned. The hot combustion gas is then expanded in the turbine section, producing rotating mechanical power to drive the compressor and the electric generator, mounted on the same shaft (single-shaft design). In a typical microturbine air to gas heat exchanger called recuperator is added to increase the overall efficiency. The recuperator uses the heat energy available in the turbine's hot exhaust gas to preheat the compressed air before the compressed air goes into the combustion chamber thereby reducing the fuel needed during the combustion process. The high-speed generator of the single shaft design usually employs a permanent magnet synchronous generator (PMSG), and requires that the high frequency AC output in the order of kHz be converted to 60 Hz (or 50 Hz) for general use. This power conditioning involves rectifying the high frequency AC to DC and then inverting the DC to 60 Hz (or 50 Hz) AC. Power electronic interfacing is a critical component in the single-shaft design and is generally designed to handle transient and voltage spikes [14].

The model presented in this thesis concentrates on the slow dynamics of the MTG system, suitable for power management of MTG combined with other types of distributed generation (DG) systems. It is reasonable, while modeling the microturbine for the above purpose, to assume that the system is operating under normal operating conditions by neglecting fast dynamics of the microturbine (e.g., start-up, shutdown, internal faults and loss of power). Also, since the electromechanical behavior of the MTG system is of main interest the recuperator is not included in the model as it only serves to increase the turbine efficiency [15].

2.4 Mathematical Representation of a Microturbine

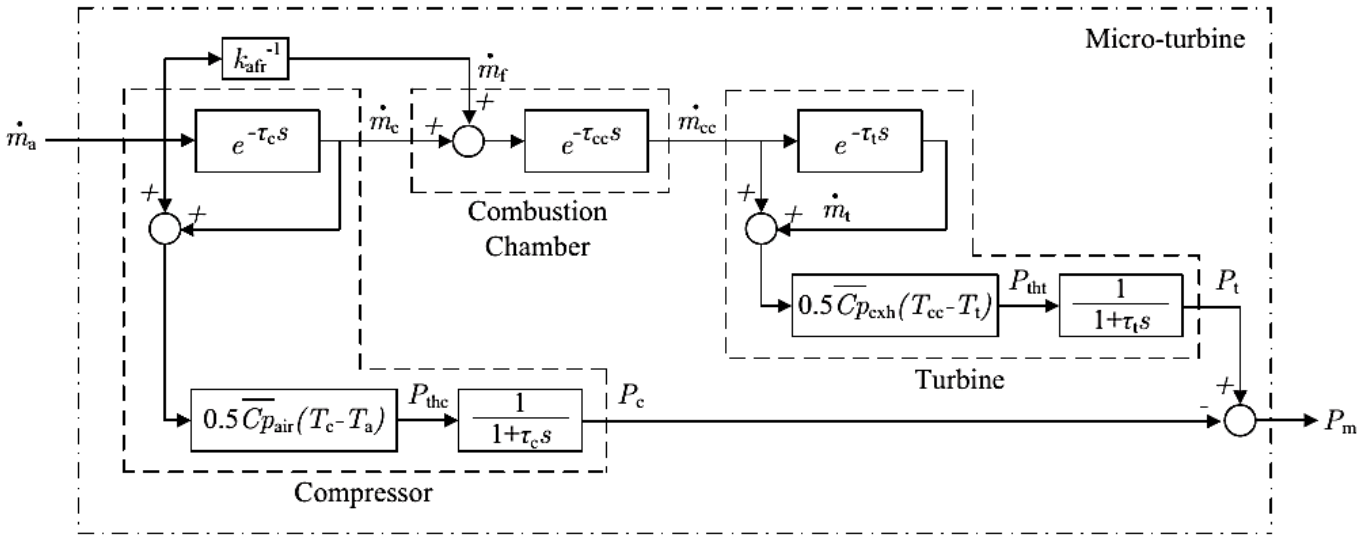

Fig. 2.2: Microturbine thermo-dynamic model

In this paper, the used microturbine model runs on validated thermodynamic data [16] and is taken from [9]. The microturbine has three thermodynamic components: a) compressor, b) combustion chamber and c) turbine. This section provides related thermo dynamic model equations with their time dependency.

The following thermodynamic equations with delays are Laplace transformed and the time delay equations having an exponential term $e^{-\tau s}$ is approximated as

$$e^{-\tau s} \approx \frac{1}{1 + s\tau}$$

which is a first order lag approximation [17].

2.4.1 Compressor:

The relationship between air mass flow rates at the compressor inlet and outlet ports is

$$\dot{m}_c(t) = \dot{m}_a(t - \tau_c) \qquad (2.1)$$

Here $\dot{m}_c(t)$ is the compressor outlet air mass flow rate, $\dot{m}_a(t)$ is the inlet air mass flow rate, and τ_c is the compressor time constant which is equal to the ratio of compressor compartment length to the mean air speed through the compartment.

The thermal power required to pressurize the inlet air is

$$P_{thc}(t) = 0.5\overline{C_{p_{air}}}[\dot{m}_a(t) + \dot{m}_c(t)]\,[T_c(t) - T_a(t)] \qquad (2.2)$$

where $P_{thc}(t)$ is the thermal power consumed by the compressor, $T_c(t)$ is the compressor outlet temperature, $T_a(t)$ is the inlet air ambient temperature, and *Cp*air is the average specific heat capacity of the inlet air between $T_a(t)$and $T_c(t)$. The specific heat capacity is not constant between state points on the micro-turbine cycle temperature-entropy diagram, but rather a function of temperature and hence *Cp*air is used to increase the accuracy in calculating $P_{thc}(t)$ [18]. This is in contrast to the thermal power calculations in [19] and [20], which both assume the inlet air specific heat capacity is constant regardless of temperature variation. When considering large temperature differentials this can introduce significant calculation errors. The mechanical power consumed by the compressor, $P_c(t)$, is related to the compressor's thermal power consumption by

$$\dot{P_c}(t) = \frac{1}{\tau_c}[P_{thc}(t) - P_c(t)] \qquad (2.3)$$

2.4.2 Combustion Chamber

The amount of fuel injected into the combustion chamber is in proportion to $\dot{m}_a(t)$

$$\dot{m}_f(t) = k_{far}\dot{m}_a(t) \quad (2.4)$$

here $\dot{m}_f(t)$ is the mass flow rate of the fuel, and k_{far} is the inlet air to fuel ratio. The fuel considered in this work is natural gas, which is a commonly utilized energy source for the Capstone C60 MicroTurbine unit. The mass flow rate at the combustion chamber outlet port is characterized by

$$\dot{m_{cc}}(t) = \dot{m}_c(t - \tau_{cc}) + \dot{m}_f(t - \tau_{cc}) \quad (2.5)$$

where $\dot{m_{cc}}(t)$ is the mass flow rate of the exhaust gas exiting the combustion chamber, and τ_{cc} is the combustion chamber time constant which is equal to the ratio of combustion chamber compartment length to the mean air speed through the compartment. It should be noted that the combustion process does not directly generate mechanical power output; it increases the energy content of the gas passing through it.

2.4.3 Turbine

The air mass flow rate at the turbine outlet is given by

$$\dot{m}_t(t) = \dot{m_{cc}}(t - \tau_t) \quad (2.6)$$

where $\dot{m}_t(t)$ is the turbine air mass flow rate, and τ_t is the turbine time constant which is equal to the ratio of turbine compartment length to the mean air speed through the compartment. The thermal power generated by the turbine is

$$P_{tht}(t) = 0.5\overline{C_{p_{exh}}}\,[\dot{m}_t(t) + \dot{m_{cc}}(t)]\,[T_{cc}(t) - T_t(t)] \quad (2.7)$$

Here $P_{tht}(t)$ is the thermal power generated by the turbine, $T_{cc}(t)$ is the combustion chamber outlet temperature, $T_t(t)$ is the turbine outlet temperature, and $C_{p_{exh}}$ is the average specific heat capacity of the exhaust gas between $T_t(t)$and $T_{cc}(t)$. Similar to the discussion regarding $C_{p_{air}}$ within (2), $C_{p_{exh}}$ accounts for the temperature dependence of the specific heat capacity. This becomes increasingly important here for reducing calculation errors as this compartment typically experiences relatively high temperature drops. Moreover, a subtle point to note is the specific heat capacities in (2) and (7) are different quantities. Compared to the strategy employed by [19] and [20] where the specific heat capacities of the inlet air and exhaust gas were assumed equal, this more accurately reflects the thermodynamic process within each compartment. The turbine generates a mechanical power output, $P_t(t)$ which is governed by

$$\dot{P_t}(t) = \frac{1}{\tau_t}[P_{tht}(t) - P_t(t)] \tag{2.9}$$

The net mechanical power output generated by the microturbine, $P_m(t)$, is the difference between the mechanical power generated by the turbine and the mechanical power consumed by the compressor

$$P_m(t) = P_t(t) - P_c(t) \tag{2.10}$$

This power output from the micro-turbine is the power exerted on the turbine shaft. For the Capstone C60 Microturbine the turbine shaft is directly coupled to a high-speed PMSG.

Chapter 3

Permanent Magnet Synchronous Generator

3.1 Permanent magnet

Magnets that keeps their magnetic fields for a long periods in varying conditions are called permanent magnet. Permanent magnets are typically not made of iron, which can lose magnetic strength over time. A type of magnet called a rare-earth magnet can be formed into shapes needed to fit inside a PMSG.

A good permanent magnet should produce a high magnetic field with a low mass, and should be stable against the influences which would demagnetize it. The desirable properties of such magnets are typically stated in terms of the remanence and coercivity of the magnet materials.

When a ferromagnetic material is magnetized in one direction, it will not relax back to zero magnetization when the imposed magnetizing field is removed. The amount of magnetization it retains at zero driving field is called its remanence. It must be driven back

to zero by a field in the opposite direction; the amount of reverse driving field required to demagnetize it is called its coercivity. If an alternating magnetic field is applied to the material, its magnetization will trace out a loop called a hysteresis loop. The lack of retrace ability of the magnetization curve is the property called hysteresis and it is related to the existence of magnetic domains in the material. Once the magnetic domains are reoriented, it takes some energy to turn them back again. This property of ferromagnetic materials is useful as a magnetic "memory". Some compositions of ferromagnetic materials will retain an imposed magnetization indefinitely and are useful as "permanent magnets".

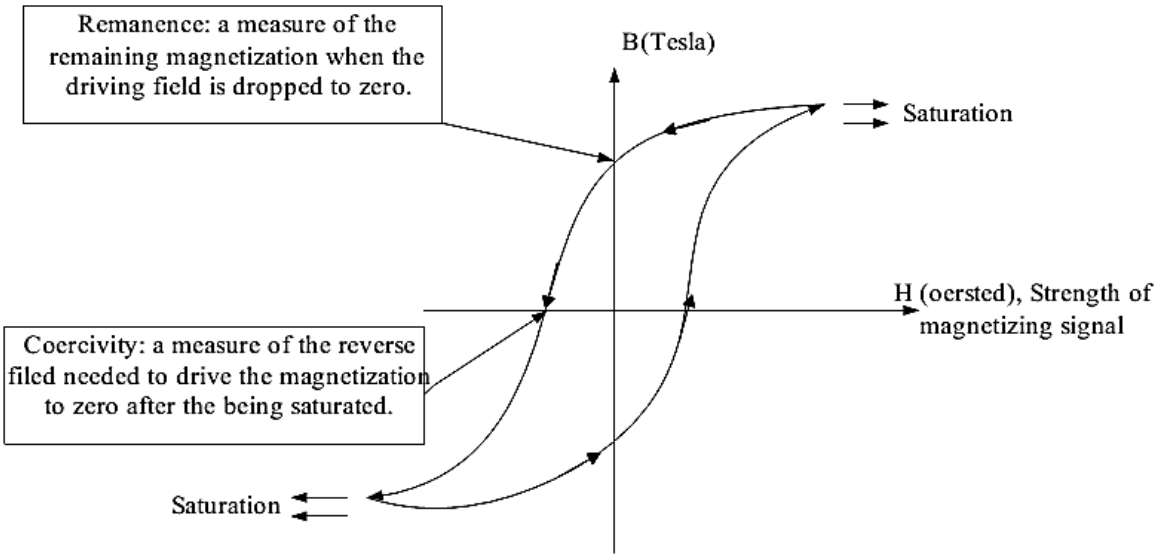

Fig 3.1: Hysteresis curve of a permanent magnet. [21]

The table below contains some data about materials used as permanent magnets. Both the coercivity and remanence are quoted in Tesla, the basic unit for magnetic field B. The hysteresis loop above is plotted in the form of magnetization M as a function of driving magnetic field strength H. This practice is commonly followed because it shows the external driving influence (H) on the horizontal axis and the response of the material (M) on the vertical axis. Besides coercivity and remanence, a quality factor for permanent magnets is the quantity (BB0/μ0) max. A high value for this quantity implies that the required magnetic flux can be obtained with a smaller volume of the material, making the device lighter and more compact.

Table 3.1: Comparison of different magnetic materials

Materials	Coercivity (T)	Remanence (T)	$(BB_0/\mu_0)_{max}$ (kJ/m^3)
$BaFe_{12}O_{19}$	0.36	0.36	25
Alnico IV	0.07	0.6	10.3
Alnico V	0.07	1.35	55
Alcomax I	0.05	1.2	27.8
MnBi	0.37	0.48	44
$Ce(CuCo)_5$	0.45	0.7	92
$SmCo_5$	1	0.83	160
Sm_2Co_{17}	0.6	1.15	215
$Nd_2Fe_{14}B$	1.2	1.2	260

Data from Myers [22]

The alloys from which permanent magnets are made are often very difficult to handle metallurgic ally. They are mechanically hard and brittle. They may be cast and then ground into shape, or even ground to a powder and formed. From powders, they may be mixed with resin binders and then compressed and heat treated. Maximum anisotropy of the material is desirable, so to that end the materials are often heat treated in the presence of a strong magnetic field.

The materials with high remanence and high coercivity from which permanent magnets are made are sometimes said to be "magnetically hard" to contrast them with the "magnetically soft" materials from which transformer cores and coils for electronics are made.

3.2 Rare Earth Magnets

The permanent magnets which have produced the largest magnetic flux with the smallest mass are the rare earth magnets based on samarium and neodymium. Their high magnetic fields and light weight make them useful for demonstrating magnetic levitation over superconducting materials.

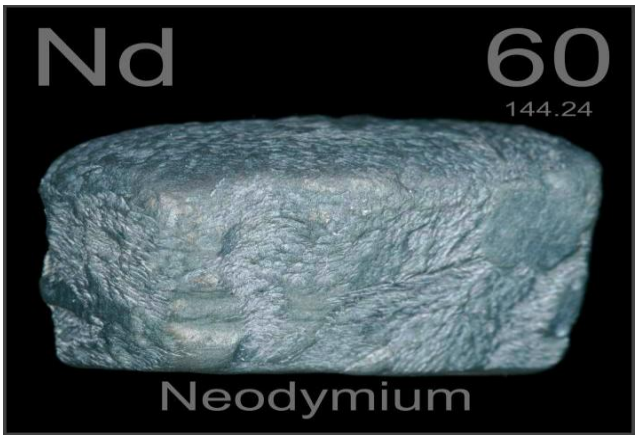

Fig 3.2: Neodymium

The samarium-cobalt combinations have been around longer, and the $SmCo_5$ magnets are produced for applications where their strength and small size offset the disadvantage of their high cost. The more recent neodymium materials like $Nd_2Fe_{14}B$ produce comparable performance, and the raw alloy materials cost about 1/10 as much. They have begun to find application in microphones and other applications that exploit their high field and light weight. The production is still quite costly since the raw alloy must be ground to powder, pressed into the desired shape and then sintered to make a durable solid [14, 23]

Table 3.2: Low cost magnetic materials comparison

Materials	Coercivity (T)	Remanence (T)	$(BB_0/\mu_0)_{max}$ (kJ/m^3)
$SmCo_5$	1	0.83	160
Sm_2Co_{17}	0.6	1.15	215
$Nd_2Fe_{14}B$	1.2	1.2	260

Data from Myers [22]

3.3 Types of permanent magnet used in PMSG

There are several types of permanent magnet used in PMSG. These are

- Alnico: Aluminum Nickel Cobalt
- Fe_3O_4: Ceramic/Ferrite
- $SmCo_5$: Samarium Cobalt
- NeFeBo: Neodymium Iron Boron

3.3.1 Alnico: Aluminum Nickel Cobalt

Alnico is an acronym referring to a family of iron alloys which in addition to iron are composed primarily of aluminum (Al), nickel (Ni) and cobalt (Co), hence al-ni-co. They also include copper, and sometimes titanium. Alnico alloys are ferromagnetic, with a high coercivity (resistance to loss of magnetism) and are used to make permanent magnets. Before the development of rare earth magnets in the 1970s, they were the strongest type of magnet. Other trade names for alloys in this family are: Alni, Alcomax, Hycomax, Columax, and Ticonal. [23]

The composition of alnico alloys is typically 8–12% Al, 15–26% Ni, 5–24% Co, up to 6% Cu, up to 1% Ti, and the balance is Fe. The development of alnico began in 1931, when T. Mishima in Japan discovered that an alloy of iron, nickel, and aluminum had a coercivity of 400 oersted (Oe; 32 kA/m), double that of the best magnet steels of the time.

3.3.2 Fe_3O_4: Ceramic/Ferrite

A ferrite is a type of ceramic compound composed of iron oxide (Fe_2O_3) combined chemically with one or more additional metallic elements. They are both electrically nonconductive and ferrimagnetic, meaning they can be magnetized or attracted to a magnet. Ferrites can be divided into two families based on their magnetic coercivity, their resistance to being demagnetized. Hard ferrites have high coercivity; they are difficult to demagnetize. They are used to make magnets, for devices such as refrigerator magnets, loudspeakers and small electric motors. Soft ferrites have low coercivity. They are used

in the electronics industry to make ferrite cores for inductors and transformers, and in various microwave components. Yogoro Kato and Takeshi Takei of the Tokyo Institute of Technology invented ferrite in 1930.

3.3.3 $SmCo_5$: Samarium Cobalt

A samarium–cobalt (SmCo) magnet, a type of rare earth magnet, is a strong permanent magnet made of an alloy of samarium and cobalt. They were developed in the early 1970s by Albert Gale and Dilip K. Das of Raytheon Corporation [23]. They are generally ranked similarly in strength to neodymium magnets, but have higher temperature ratings and higher coercivity. They are brittle, and prone to cracking and chipping. Samarium–cobalt magnets have maximum energy products (BH_{max}) that range from 16 megagauss-oersteds (MGOe) to 33 MGOe, that is approx. 128 kJ/m^3 to 264 kJ/m^3; their theoretical limit is 34 MGOe, about 272 kJ/m^3. They are available in two "series", namely Series 1:5 and Series 2:17.

Sintered Samarium Cobalt magnets exhibit magnetic anisotropy, meaning they can only be magnetized in the axis of their magnetic orientation. This is done by aligning the crystal structure of the material during the manufacturing process.

These samarium–cobalt magnet alloys (generally written as $SmCo_5$, or SmCo Series 1:5) have one atom of rare earth samarium and five atoms of cobalt. By weight this magnet alloy will typically contain 36% samarium with the balance cobalt. The energy products of these samarium–cobalt alloys range from 16 MGOe to 25 MGOe, what is approx. 128 kJ/m^3 - 200 kJ/m^3. These samarium–cobalt magnets generally have a reversible temperature coefficient of -0.05%/°C. Saturation magnetization can be achieved with a moderate magnetizing field. This series of magnet is easier to calibrate to a specific magnetic field than the SmCo 2:17 series magnets.

In the presence of a moderately strong magnetic field, non-magnetized magnets of this series will try to align their orientation axis to the magnetic field, thus becoming slightly magnetized. This can be an issue if post-processing requires that the magnet be plated or coated. The slight field that the magnet picks up can attract debris during the plating or

coating process, causing coating failure or a mechanically out-of-tolerance condition. Samarium - cobalt magnet has a strong resistance to corrosion and oxidation resistance, usually do not need to be coated can be widely used in high temperature and poor working conditions.

3.3.4 NeFeBo: Neodymium Iron Boron

Sintered neodymium-iron-boron (NdFeB) magnets, also referred to as "neo" magnets, have been commercially available since November 1984. They offer the highest energy product of any material today and are available in a very wide range of shapes, sizes and grades. Earliest use of neo magnets was primarily for voice coil motors (VCM's) in hard disk drives and this market still accounts for about 55% of total sales dollars. Other applications include high performance motors, brushless DC motors, magnetic separation, magnetic resonance imaging, sensors and loudspeakers.

3.4 Permanent Magnet Synchronous Generator

A generator where the excitation field is provided by a permanent magnet instead of a coil is permanent magnet synchronous generator (PMSG).

A direct drive wind energy systems cannot employ a conventional high speed (and low torque) electrical machines. Hartkopf et al. The weight and size of electrical machines increases when the torque rating increases for the same active power. Therefore, it is essential task of the machine designer to consider an electrical machine with high torque density, in order to minimize the weight and the size. In and it has been shown that PM synchronous machines have higher torque density compared with induction and switched reluctance machines. Thus a PMSG is chosen for further studies in this work. However, since the cost effectiveness of PMSG is an important issue, low manufacturing cost has to be considered as a design criterion in further steps. There are a number of different PMSG topologies; some of them are very attractive from the technical point of view. However, some of the state of the art topologies suffer from complication in manufacturing process which results in high production costs. PM

excitation offers many different solutions. The shape, the size, the position, and the orientation of the magnetization direction can be arranged in many different ways. Here, presented topologies include those of which are investigated for low speed applications or variable speed applications. This list encompasses radial or axial flux machines, longitudinal or transversal flux machines, inner rotor or outer rotor machines and interior magnet or exterior magnet machines. Slot less machines are not presented here.

As the construction basis PM synchronous machine describe as follow:

i. Stator
ii. Rotor

There are some different types of rotors. These are:

a. Axial and radial flux rotor

b. Longitudinal or Transversal rotor

c. Inner Rotor or Outer Rotor

3.5 Rotor mechanism

Air gap orientation can be identified in two different ways. Here a hypothetical normal vector to the air gap is adopted along the flux direction. The axis of the machines is assumed to be along the length of the machine in the cylindrical coordinate system. Relation of the normal vector with the axis of the machine decides the radial or axial topology. If the normal vector is perpendicular to axis, machine is called radial. If the normal vector is parallel with the axis, the machine is called axial.

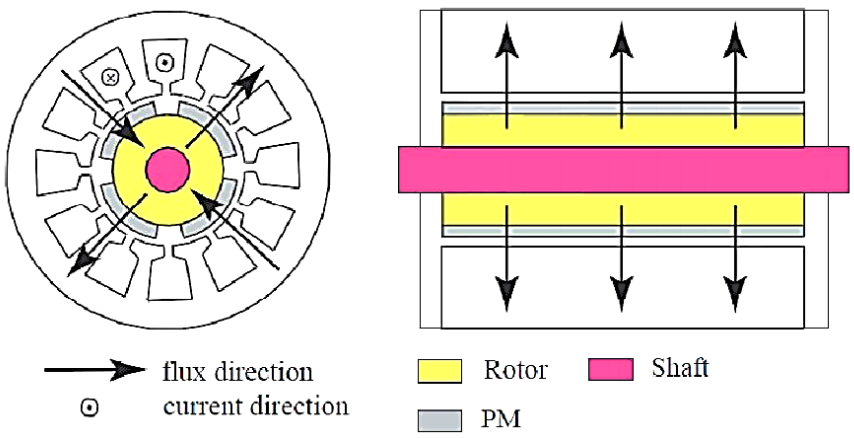

Fig 3.3: Cross sectional view in radial direction and in axial direction, respectively, of a typical radial flux PMSG.

3.5.1 Radial Flux Machines

Radial flux machines are conventional type of PMSG. The manufacturing technology is well established which makes the production cost lower compared with the axial one. Furthermore, they are very flexible for scaling, as the higher power ratings of the machine are achieved by increasing the length of the machine. In other words completely new design and completely new geometry can be avoided. They are extensively used in ship propulsion, robotics, traction and wind systems. Fig. 3.3 shows cross sectional view in radial direction and in axial direction, respectively, of a typical radial flux PMSG.

3.5.2 Axial Flux Machines

Various axial flux topologies have been proposed in recent years and their pros and cons are categorized. Generally, in axial flux machines length of the machine is much smaller compared with radial flux machines. Their main advantage is high torque density, so they are recommended for applications with size constraints especially in axial direction. They have found application in gearless elevator systems, and they are rarely used in traction, servo application, micro generation and propulsion systems . Figure 3.3 shows cross sectional view in radial direction and in axial direction, respectively, of a

typical axial flux PMSG . One of the disadvantages with the axial flux machines is that they are not balanced in single rotor single stator edition. Usually, for a better performance the rotor is sandwiched between two stators or vice versa.

3.5.3 Longitudinal or Transversal

In transversal flux machines, the plane of flux path is perpendicular to the direction of rotor motion. The use of transversal flux machines can be proposed in applications with high torque density requirement. One attractive property of the transversal flux machines is that the current loading and the magnetic loading can be adjusted independently. They are proposed for wind systems, free piston generators for hybrid vehicles and ship propulsion.

3.5.4 Inner Rotor or Outer Rotor

The rotor surrounds the stator in outer rotor machines. In these machines, the magnets are usually located on the inner circumference of the rotor. Accordingly, for the same outer diameter of the machine, in the outer rotor machine the rotor has higher radius compared with the stator and it can be equipped with higher number of poles for the same pole pitch. Another advantage is that the magnets are well supported despite the centrifugal force.

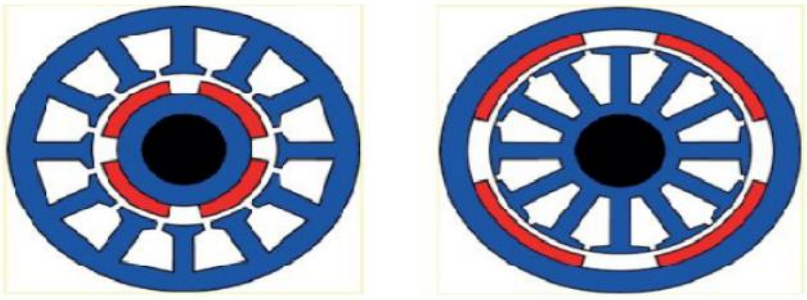

Fig 3.4: Inner rotor PMSG (left) and an outer rotor PMSG (right).

However, the inner rotor machines are a more common solution present on the market today. In small machines, the main contributions to the losses are copper losses and therefore the stator winding has the highest temperature rise in the active material of the machine. Hence, it is more beneficial to put the stator winding, rather than the magnets, closer to the housing, where the cooling properties are good. This causes less temperature rise for the same amount of losses. Fig. 3.4 shows an inner rotor PMSG and an outer rotor PMSG.

3.6 Operating Region of a PMSM

Fig. 3.5 shows the demagnetization segment of the B-H curve where the permanent magnet is usually designed to operate [24].

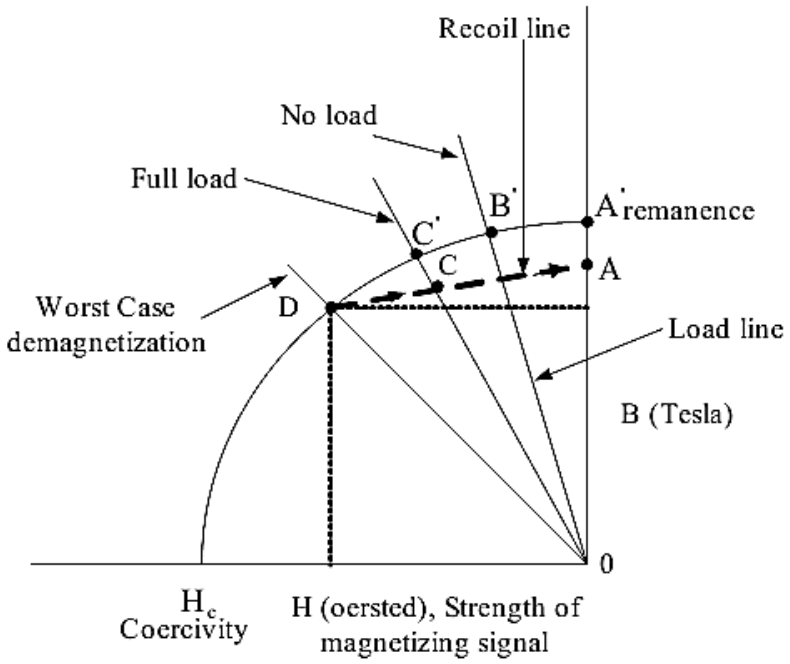

Fig.3.5: Permanent magnet machine operating points on B-H curve.

The maximum flux density Br corresponding to A' will be available initially (no air-gap). When the magnet is installed in the machine, the air gap will have some demagnetization effect and the operating point B' correspond to the no-load line as shown in Fig. 3.5. When

current flows in the stator winding, the magnetic axis (direct axis) armature reaction effect can have further demagnetization effect, which will reduce the air gap flux density further.

A load line representing worst-case demagnetization (may be due to starting, transient or machine fault condition) is also shown in Fig. 3.5.

Once the operating point reaches the D and the demagnetization effect is removed, the magnet will recover along the recoil line (DA). Subsequently, the stable operating point will be determined by the intersection of the load line and the recoil line. The magnet is therefore permanently demagnetized at no-load operation, corresponding to the vertical distance between A' and A. If the permanent magnet material has a straight-line demagnetization curve, the recoil line will coincide with the demagnetization line irrespective of the worst case magnetization point (i.e., permanent demagnetization will be negligible). The characteristics for several possible permanent magnet materials are given in reference [24].

3.7 *dq*-Axis Representation of a PMSM

In a PMSM, the permanent magnets are glued on the rotor in surface sinusoidal magnet machine (SPM), and are mounted inside the rotor in case of an interior or buried magnet synchronous machine (IPM). The stator has three phase sinusoidal winding, which creates a synchronously rotating air gap flux. If the machine is rotated by a prime mover, the stator windings generate balanced three-phase sinusoidal voltages. The *dq* axis representation of a permanent magnet synchronous machine (for a balanced system the 0-axis quantities are equal to zero), where is shown in the Fig. 3.6 [24], [25], [26]. In this figure the finite core loss is represented by the dotted damper windings.

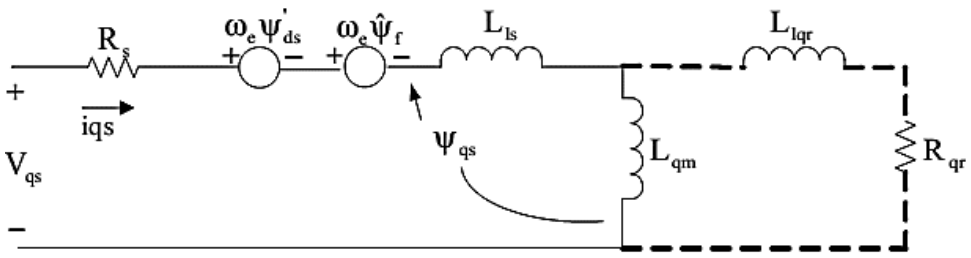

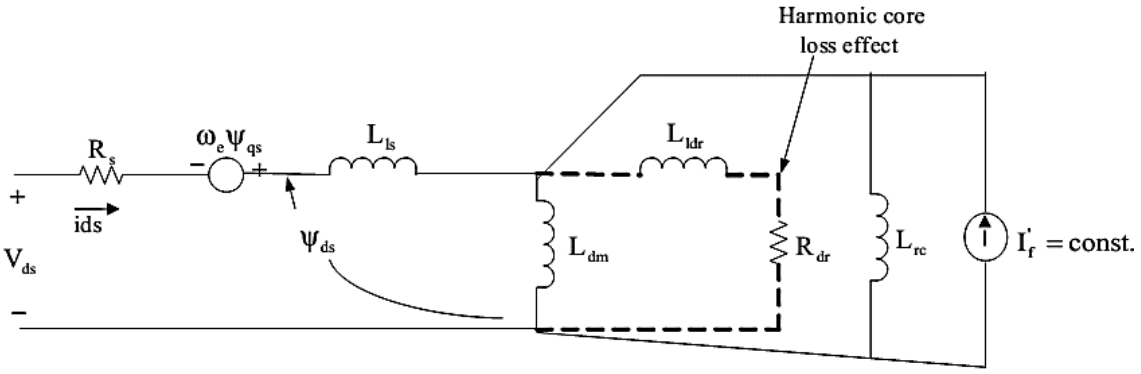

Fig. 3.6: Synchronously rotating frame equivalent circuits of a PMSM.

Ignoring core loss, the circuit equations can be written as (equations are valid for both IPM as well as SPM (for SPM L_{dm}=L_{qm})

$$V_{qs} = R_s i_{qs} + \omega_e \psi'_{ds} + \omega_e \psi_f + \frac{d\psi_{qs}}{dt} \tag{3.1}$$

$$V_{ds} = R_s i_{ds} - \omega_e \psi_{qs} + \frac{d\psi_{ds}}{dt} \tag{3.2}$$

where the flux linkages are given by the following equations:

$$\psi_f = L_{dm} I'_f \tag{3.3}$$

$$\psi'_{ds} = i_{ds}(L_{ls} + L_{dm}) = i_{ds} l_{ds} \tag{3.4}$$

$$\psi_{ds} = \psi_f + \psi'_{ds} \tag{3.5}$$

$$\psi_{qs} = i_{qs}(L_{ls} + L_{qm}) = i_{qs} L_{qs} \tag{3.6}$$

The electromagnetic developed in the machine air gap is given by:

$$T_e = \frac{3}{2} \times \frac{P}{2}(\psi_{ds} i_{qs} - \psi_{qs} i_{ds}) \tag{3.7}$$

Substituting (3.1)-(3.5) in (3.3), (3.4) and (3.7) and simplifying, we have

$$\frac{di_{qs}}{dt} = \frac{1}{L_{qs}} [V_{qs} - R_s i_{qs} - L_{ds} w_e i_{ds} - \psi_f w_e] \tag{3.8}$$

$$\frac{di_{ds}}{dt} = \frac{1}{L_{ds}} [V_{ds} - R_s i_{ds} + w_e L_{qs} i_{qs}] \tag{3.9}$$

$$T_e = \frac{3P}{4}[\psi_f i_{qs} + (L_{ds} - L_{qs}) i_{qs} i_{ds}] \quad (3.10)$$

The rotor speed is obtained from the dynamics of the mechanical system as follows:

$$\frac{d\omega_r}{dt} = \frac{1}{J}(T_e - T_{shaft}) \quad (3.11)$$

where ω_e, ω_r are electrical and mechanical angular velocities of the rotor (rad/sec), V_{qs}, $V_{ds}(i_{qs}, i_{ds})$ are q and d axis voltage (current) components and L_{qs} and L_{ds} are q and d axis inductances of the stator respectively. L_{dm} is the common d-axis mutual inductance of the stator lumped with the damper windings and the permanent magnet inductance L_{rc} (associated with the recoil slope).

I_f is an equivalent field current of the permanent magnets and I'_f is its equivalent referred to the stator side,

$\psi_f(\psi_f = L_{dm} I'_f = constant)$ denotes flux linkage induced by the permanent magnets of the rotor in stator phases,

J is the inertia of the rotor (Kgm^2)

T_{shaft} is the shaft torque produced by the microturbine (Nm),

T_e is the electric torque generated by the PMSG (Nm), and

P is the number of poles.

Note that the signs for the generated torque T_e and shaft torque T_{shaft} are positive for motor operation and negative for generator operation.

Chapter 4

Power Conditioning System

4.1 Introduction

As discussed, single-shaft Microturbines require power conditioning system to convert the high frequency AC power produced by the generator into usable electricity. The power conditioning system is actually an AC-DC-AC converter. This is comprised of an AC-to-DC rectifier and a DC-to-AC inverter. It consists of 2 parts:

1. AC-to-DC Rectifier
2. DC-to-AC Inverter

The high frequency AC is, at first, rectified to DC and then inverted back to 50 or 60 Hz of AC. Power Conditioning System matches the generated electricity with the grid frequency.

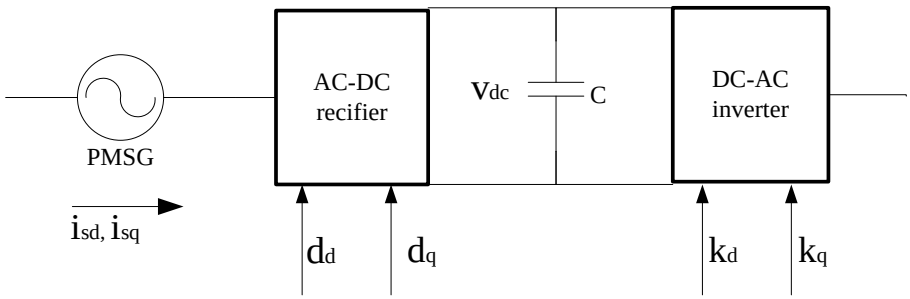

Fig. 4.1: Power Conditioning System

4.2 AC-to-DC Rectifier

AC-to-DC Rectifier converts the generated high frequency AC electricity to DC.

4.2.1 Circuit Diagram & Dynamic Equations

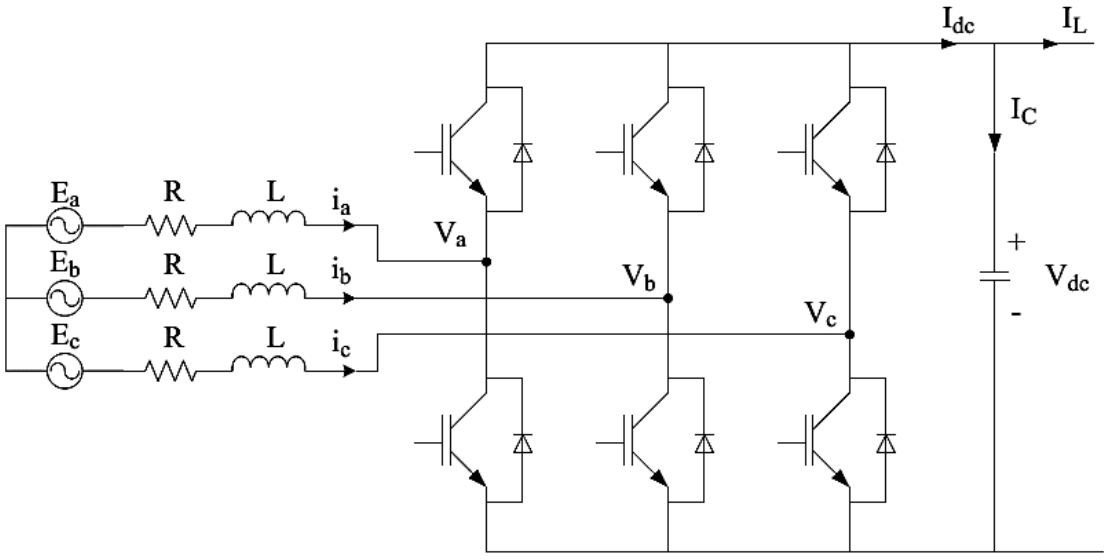

Fig 4.2: AC-to-DC Rectifier

A three-phase grid-connected system is shown in Fig. 4.2, R is the line resistance, L is combination of filter and line inductance, i is the current injected into the grid, v is the

voltage of the DC-link and e is the grid voltage, ω = 2πf is the angular frequency and f = 50 Hz is the grid frequency [27]. Now, by applying KCL at the node where the DC-link is connected as shown in Fig. 4.2, we get

$$I_{dc} = I_c + I_L \tag{4.1}$$

where I_{dc} is the input current of the inverter and $I_c = C\frac{dv}{dt}$ is the current flowing through the capacitor [28]. After doing some simplifications, equation (4.1) can be written in the following form:

$$\frac{dv}{dt} = \frac{1}{C}(I_{dc} - I_L) \tag{4.2}$$

The following equations relate the *d* and *q*-axis stator output voltages with rectifier DC output voltage.

$$L\frac{di_{ds}}{dt} = -Ri_{ds} + \omega i_{qs} + v_{sd} - d_d v_{DC} \tag{4.3}$$

$$L\frac{di_{qs}}{dt} = -Ri_{qs} - \omega i_{ds} + v_{sq} - d_q v_{DC} \tag{4.4}$$

where, *L* and *R* are the inductance and resistance of the conductor between PMSG and AC-to-DC converter, d_d and d_q are the switching parameters of rectifier, respectively and v_{DC} is the rectifier output DC voltage.

Considering small length, ideal conductor, *L*= 0 and *R* = 0, following equations can be achieved.

$$v_{sd} = d_d v_{DC} \tag{4.4}$$

$$v_{sq} = d_q v_{DC} \tag{4.6}$$

4.2.2 Generating Switching Parameters

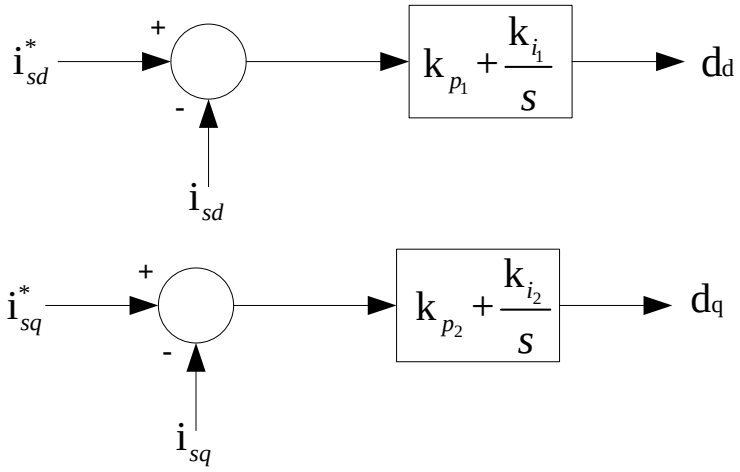

Fig.4.3: Control Block Diagrams for the switching parameters of DC-to-AC Inverter.

Fig 4.3 shows that the switching parameters of AC-to-DC converters are controlled by the stator currents deviation of the PMSG.

4.3 DC-to-AC Inverter

DC-to-AC Inverter converts the DC link voltage to AC electricity of desired frequency of 50 Hz or 60 Hz

4.3.1 Circuit Diagram & Dynamic Equations

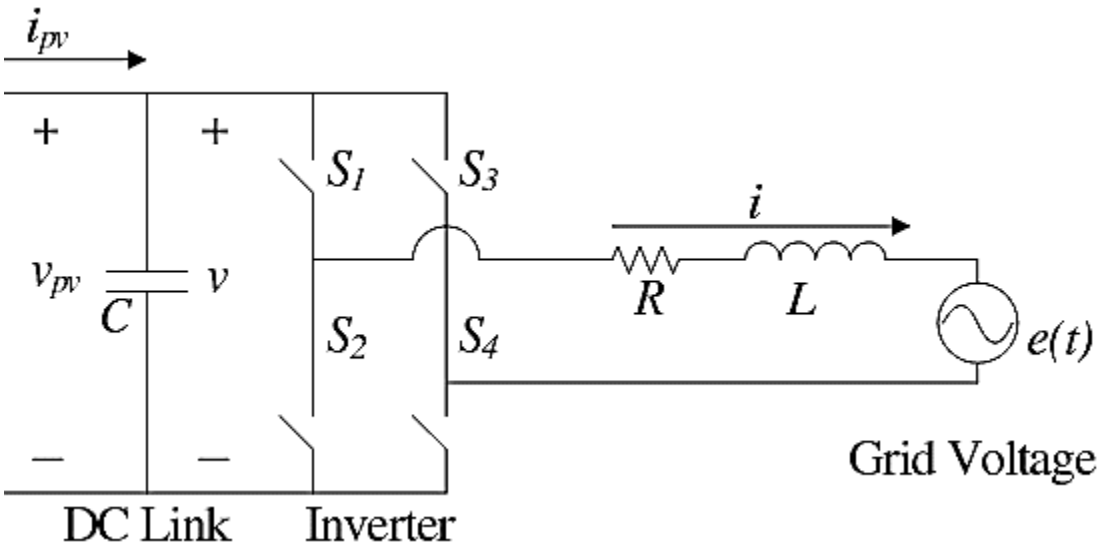

Fig 4.4: DC-to-AC Inverter

In Fig. 4.4, S1, S2, S3, and S4 are the four switches of the inverter, R is the line resistance, L is combination of filter and line inductance, i is the current injected into the grid, v is the voltage of the DC-link and e is the grid voltage, ω = 2πf is the angular frequency and f = 50 Hz is the grid frequency [28]. Now, by applying KCL at the node where the DC-link is connected as shown in Fig. 4.4, we get

$$i_{\mathrm{pv}} = i_{\mathrm{dc}} + i_{\mathrm{C}} \tag{4.3}$$

where i_{dc} is the input current of the inverter and $i_c = C\frac{dv}{dt}$ is the current flowing through the capacitor. After doing some simplifications, equation (4.3) can be written in the following form:

$$\frac{dv}{dt} = \frac{1}{C}\left(i_{\mathrm{pv}} - i_{\mathrm{dc}}\right) \tag{4.4}$$

Since i_{dc} is the input current of the inverter, in terms of the output current i of the inverter it can be written as follows:

$$i_{\mathrm{dc}} = \vec{m}\,\vec{i} \tag{4.4}$$

where $\vec{m}$ represents the space-phasor corresponding to the pulse width modulation (PWM) signals which are normalized to the peak value of the triangular carrier $\vec{i}$ signal, is the phasor representation of i, and $i_{\mathrm{dc}} = |m||i|$. Finally, equation (4.4) can be written as

$$\frac{dv}{dt} = \frac{1}{C}\left(i_{\mathrm{pv}} - \vec{m}\,\vec{i}\right) \tag{4.6}$$

Now, by applying KVL at the AC side of the inverter as shown in Fig. 4.4, it can be written that

$$\vec{v}_{\mathrm{out}} = R\vec{i} + L\frac{d\vec{i}}{dt} + \vec{e} \tag{4.7}$$

where → represents the phasor quantity of the corresponding variables. In terms of input DC voltage v of the inverter the output AC $\vec{v}_{\mathrm{out}}$ voltage can be expressed as follows:

$$v_{\mathrm{out}} = \vec{m}v \tag{4.8}$$

Using the above relation, equation (4.7) can be simplified as follows:

$$\frac{d\vec{i}}{dt} = \frac{1}{L}\left(\vec{m}v - R\vec{i} - \vec{e}\right) \tag{4.9}$$

For analysis and control purposes, space-phasor variables can be projected on a *dq*-frame which can be achieved by replacing each space-phasor by its *dq*-frame equivalent as

$$\overrightarrow{x} = (X_{\mathrm{d}} + jX_{\mathrm{q}})\, e^{j\omega t} \tag{4.10}$$

If $\overrightarrow{x}$ represents a state variable, then

$$\frac{d\overrightarrow{x}}{dt} = \left(\frac{dX_{\mathrm{d}}}{dt} + j\frac{dX_{\mathrm{q}}}{dt}\right) e^{j\omega t} + \omega\,(X_{\mathrm{d}} + jX_{\mathrm{q}})\, e^{j\omega t} \tag{4.11}$$

where ω is the *dq*-frame angular frequency. The space-phasor to *dq*-frame can be obtained by using the following relation:

$$(X_{\mathrm{d}} + jX_{\mathrm{q}}) = \overrightarrow{x} e^{-j\omega t} \tag{4.12}$$

Using the relations presented by equations (4.10)-(4.12), the system model represented by equations (4.9) and (4.9) can be transformed into the following *dq*-frame:

$$\begin{aligned}
\dot{I}_{\mathrm{d}} &= -\frac{R}{L} I_{\mathrm{d}} + \omega I_{\mathrm{q}} - \frac{E_{\mathrm{d}}}{L} + \frac{v}{L} M_{\mathrm{d}} \\
\dot{I}_{\mathrm{q}} &= -\omega I_{\mathrm{d}} - \frac{R}{L} I_{\mathrm{q}} - \frac{E_{\mathrm{q}}}{L} + \frac{v}{L} M_{\mathrm{q}} \\
\dot{v}_{\mathrm{pv}} &= \frac{1}{C} i_{\mathrm{pv}} - \frac{1}{C} I_{\mathrm{d}} M_{\mathrm{d}} - \frac{1}{C} I_{\mathrm{q}} M_{\mathrm{q}}
\end{aligned} \tag{4.13}$$

Equations (4.13) represent the complete mathematical model of the single-phase grid-connected MTG system which is nonlinear due to the switching functions and diode current. In equations (4.13), M_d and M_q are the control inputs and the output variables are I_q and v. A three-phase grid-connected MTG system is shown in Fig. 4.4 in which S1, S2, S3, S4, S4, and S6 are the six switches of the inverter. In the state-space form, Fig. 4.4 can be represented through the following equations

$$\begin{aligned}
\dot{i}_a &= -\frac{R}{L}i_a - \frac{1}{L}e_a + \frac{v_{pv}}{3L}(2K_a - K_b - K_c) \\
\dot{i}_b &= -\frac{R}{L}i_b - \frac{1}{L}e_b + \frac{v_{pv}}{3L}(-K_a + 2K_b - K_c) \\
\dot{i}_c &= -\frac{R}{L}i_c - \frac{1}{L}e_c + \frac{v_{pv}}{3L}(-K_a - K_b + 2K_c)
\end{aligned} \tag{4.14}$$

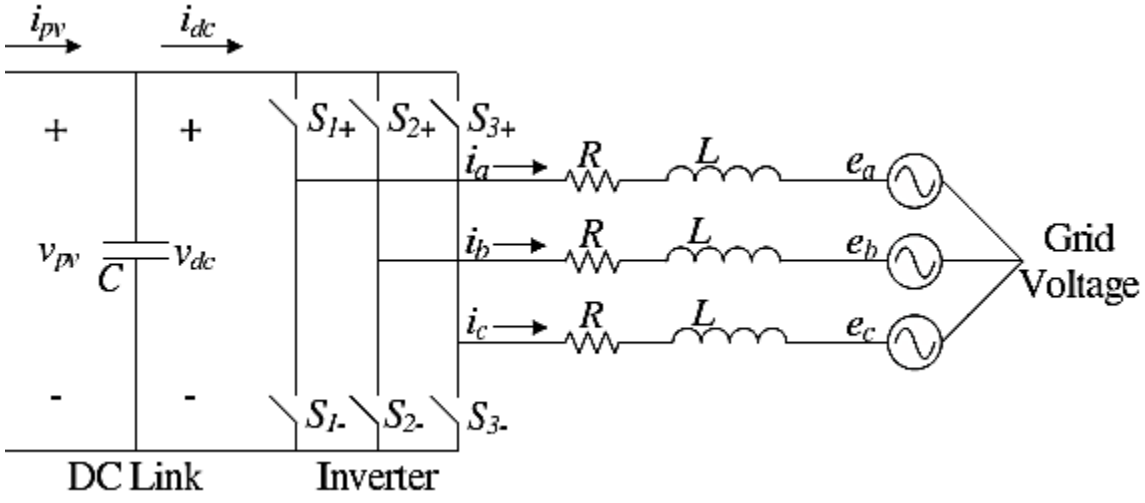

Fig 4.5: Three-Phase DC-to-AC Inverter

where K_a, K_b, and K_c are the input switching signals. Now, by applying KCL at the node where the DC link is connected, we obtain

$$\dot{v}_{pv} = \frac{1}{C}\left(i_{pv} - i_{dc}\right) \tag{4.14}$$

But the input current of the inverter i_{dc} can be written as [61,62]

$$i_{dc} = i_a K_a + i_b K_b + i_c K_c \tag{4.16}$$

which yields

$$\dot{v}_{pv} = \frac{1}{C} i_{pv} - \frac{1}{C}\left(i_a K_a + i_b K_b + i_c K_c\right) \tag{4.17}$$

The complete model of a three-phase grid-connected MTG system can be presented by equations (4.14) and (4.17) which are nonlinear and time variant and can be converted into a time invariant model by applying *dq* transformation using the angular frequency (ω) of the grid, rotating reference frame synchronized with grid where the *d* component of the grid voltage Ed is zero [29, 30]. By using *dq* transformation, from equations (4.14) and (4.17), the following equations can be written

$$\frac{di_{gd}}{dt} = -\frac{v_{gd}}{L_g} - \frac{R_g i_{gd}}{L_g} + \frac{v_{dc} k_d}{L_g} + \omega i_{gq} \tag{4.18}$$

$$\frac{di_{gq}}{dt} = -\frac{v_{gq}}{L_g} - \frac{R_g i_{gq}}{L_g} + \frac{v_{dc} k_q}{L_g} - \omega i_{gd} \tag{4.19}$$

$$\frac{dv_{dc}}{dt} = \frac{1}{C}\left[d_d i_{sd} + d_q i_{sq} - \left(k_d i_{sd} + k_q i_{sq}\right)\right] \tag{4.20}$$

where, i_{gd} and i_{gq} are the *d* and *q*-axis distribution side currents, respectively, v_{gd} and v_{gq} are the *d* and *q*-axis distribution side voltages, respectively, R_g is the distribution side resistance, L_g is the distribution side inductance, k_d and k_q are the switching parameters of the inverter, respectively, and *C* is the capacitance of the capacitor between the rectifier and the inverter.

4.3.2 Generating Switching Parameters:

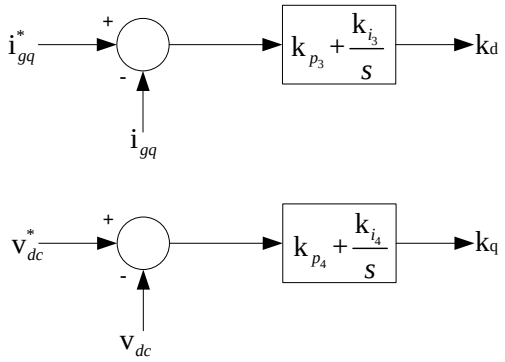

Fig.4.6: Control Block Diagrams for the switching parameters of DC-to-AC Inverter.

The switching parameters of the of the DC-to-AC inverter shown in Fig. 4.6 are controlled by the q-axis grid side current deviation and voltage deviation of the DC-link, respectively.

Chapter 5

Genetic Algorithm

5.1 Introduction

For controlling purpose, PI controllers have been used in different parts of the system. The PI controller parameters are selected by an optimizing toolbox in MATLAB called Genetic Algorithm (GA) for optimal tuning.

The GA procedure is based on the Darwinian principle of survival of the fittest [31]. It is a technique to solve both constrained and unconstrained optimization problems based on a natural selection process that mimics biological evolution. An initial population is created containing a predefined number of individuals or solutions, each represented by a genetic string incorporating the variable information. The algorithm selects individuals from the current generation for reproduction or crossover at each generation with an appropriate mutation factor to develop the next generation. Over successive generations, the population evolves towards an optimal solution. To determine when to stop, the algorithm uses some predefined conditions i.e. generations, time limit, fitness limit, stall generations, stall time limit etc. The algorithm stops as soon as any one of the conditions are met. A range of values might be given to the algorithm for more appropriate results [32].

5.2 Outline of the Algorithm

The following outline summarizes how the genetic algorithm works [32]:

1. The algorithm begins by creating a random initial population.
2. The algorithm then creates a sequence of new populations. At each step, the algorithm uses the individuals in the current generation to create the next population. To create the new population, the algorithm performs the following steps:
    a. Scores each member of the current population by computing its fitness value.
    b. Scales the raw fitness scores to convert them into a more usable range of values.
    c. Selects members, called parents, based on their fitness.
    d. Some of the individuals in the current population that have lower fitness are chosen as *elite*. These elite individuals are passed to the next population.
    e. Produces children from the parents. Children are produced either by making random changes to a single parent—*mutation*—or by combining the vector entries of a pair of parents—*crossover*.
    f. Replaces the current population with the children to form the next generation.
3. The algorithm stops when one of the stopping criteria is met.

5.3 Creating the Next Generation

At each step, the genetic algorithm uses the current population to create the children that make up the next generation. The algorithm selects a group of individuals in the current population, called *parents*, who contribute their *genes* the entries of their vectors—to their children. The algorithm usually selects individuals that have better fitness values as parents [32]. You can specify the function that the algorithm uses to select the parents in the Selection function field in the Selection options. The genetic algorithm creates three types of children for the next generation:

- *Elite children* are the individuals in the current generation with the best fitness values. These individuals automatically survive to the next generation.
- *Crossover children* are created by combining the vectors of a pair of parents.
- *Mutation children* are created by introducing random changes, or mutations, to a single parent. The following schematic diagram illustrates the three types of children.

The following sections explain how the algorithm creates crossover and mutation children.

- **Crossover Children:** The algorithm creates crossover children by combining pairs of parents in the current population. At each coordinate of the child vector, the default crossover function randomly selects an entry, or *gene*, at the same coordinate from one of the two parents and assigns it to the child. For problems with linear constraints, the default crossover function creates the child as a random weighted average of the parents.
- **Mutation Children**: The algorithm creates mutation children by randomly changing the genes of individual parents. By default, for unconstrained problems the algorithm adds a random vector from a Gaussian distribution to the parent. For bounded or linearly constrained problems, the child remains feasible.

5.4 Flow Chart of Genetic Algorithm

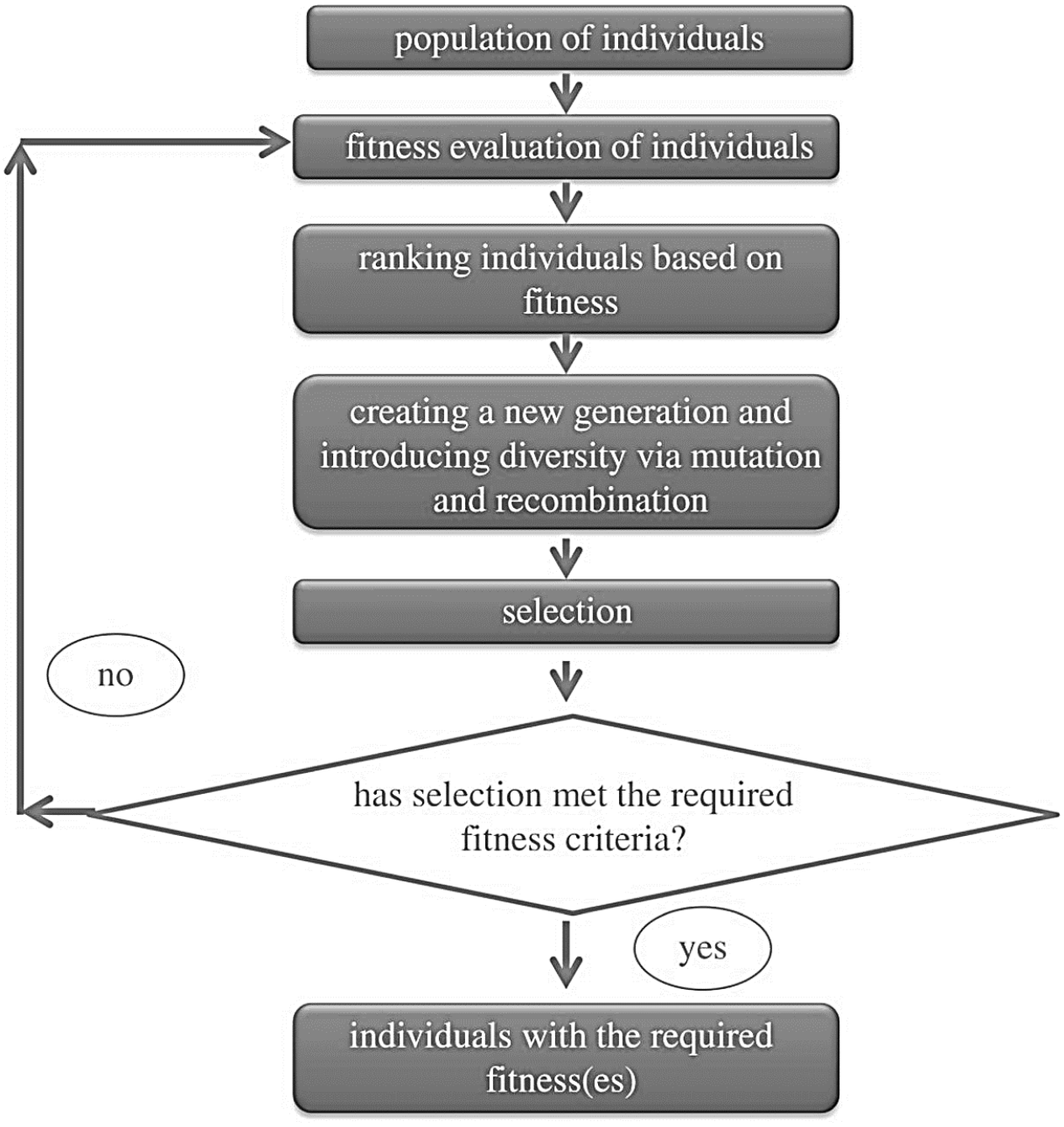

Fig. 5.1 Flow chart of GA [33]

5.5 Stopping Conditions for the Algorithm

The genetic algorithm uses the following conditions to determine when to stop:

Generations — The algorithm stops when the number of generations reaches the value of Generations.

Time limit — The algorithm stops after running for an amount of time in seconds equal to Time limit.

Fitness limit — The algorithm stops when the value of the fitness function for the best point in the current population is less than or equal to Fitness limit.

Stall generations — The algorithm stops when the average relative change in the fitness function value over Stall generations is less than Function tolerance.

Stall time limit — The algorithm stops if there is no improvement in the objective function during an interval of time in seconds equal to Stall time limit.

Stall test — The stall condition is either average change or geometric weighted. For geometric weighted, the weighting function is 1/2, where n is the number of generations prior to the current. Both stall conditions apply to the relative change in the fitness function over Stall generations.

Function Tolerance — The algorithm runs until the average relative change in the fitness function value over Stall generations is less than Function tolerance.

Nonlinear constraint tolerance — The Nonlinear constraint tolerance is not used as stopping criterion. It is used to determine the feasibility with respect to nonlinear constraints. Also, a point is feasible with respect to linear constraints when the constraint violation is below the square root of nonlinear constraint tolerance.

5.5 Conditions Used

For optimizing controller parameters, the following conditions are considered.

- Population size: 40
- Generations: 70
- Type of Selection: Roulette
- Type of Mutation: Adaptive Feasible
- Type of Crossover: Arithmetic
- Stopping Criteria: Stall Generations.

5.7 Proposed PI controller parameters using GA

Table 5.1: Proposed PI controller parameters using GA

Parameters	Values
K_{p1}	5.0985
K_{p2}	2.0984
K_{p3}	-0.90
K_{p4}	-1.9990
K_{i1}	7.0925
K_{i2}	10.0712
K_{i3}	-0.8999
K_{i4}	-0.50

Chapter 6

Simulation Results

6.1 Closed-Loop Response of Standalone Microturbine

A PI controller can be used, as shown in Fig. 6.1, to regulate the microturbine's output power. The value of the parameters K and a are determined as $7 \times 10^{-7} kg/J$ and $1200\ kg/Js$, respectively [9].

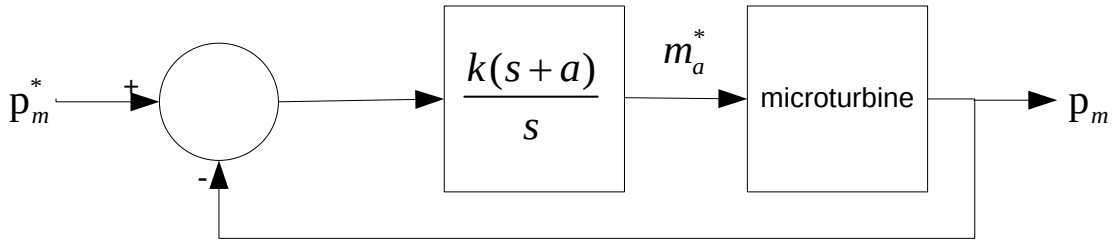

Fig. 6.1: Microturbine Control System

Fig. 6.2 illustrates the closed loop response of Pm to a step change in Pm*. Figure shows that the overshoot and rise time is very small and it reaches steady-state within a very short time.

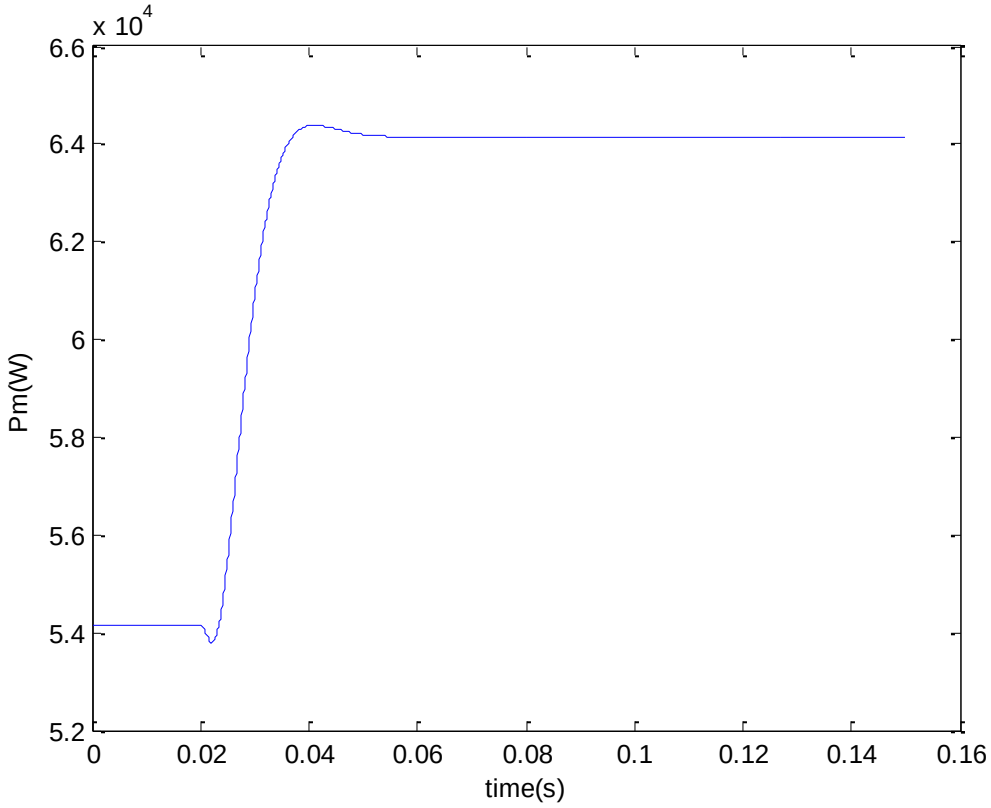

Fig.6.2: Microturbine output power closed loop step response.

6.2 Grid Connected Mode

In this simulation mode, the MTG system is connected to a distribution system. Initially, the system is operating at no load. At $t = 1\ second$, a load of 10kW is applied to the MTG system. Fig. 6.3 shows the input air flow rate for the applied load. Initially, the input air flow rate is 0.3526 p.u until the load is applied to the system at $t = 1\ second$. The new input air flow rate is 0.418 p.u.

Fig. 6.4 shows compressor output air flow rate. Due to the application of load at $t = 1\ second$, its changes are same as the input air flow rate.

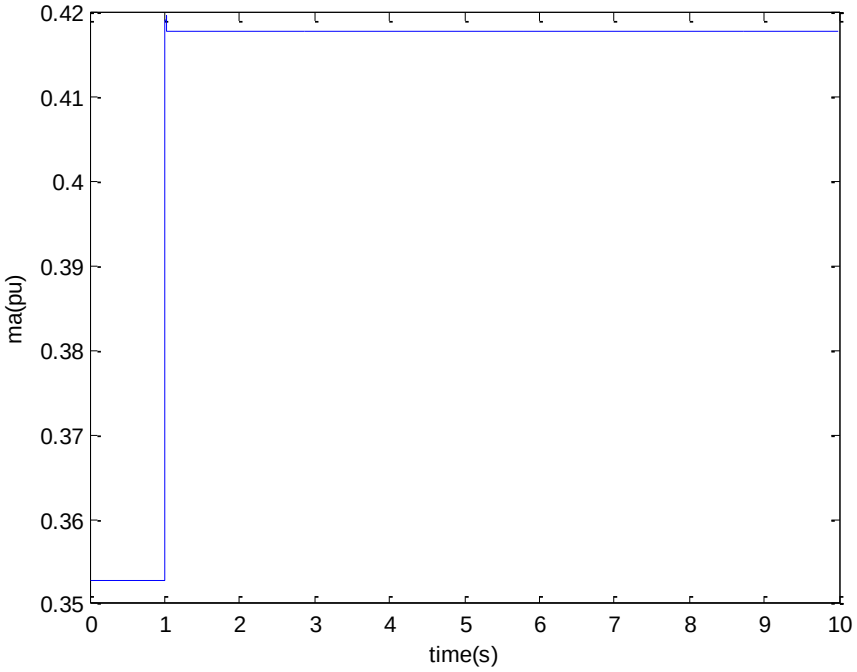

Fig.6.3: compressor input air flow rate

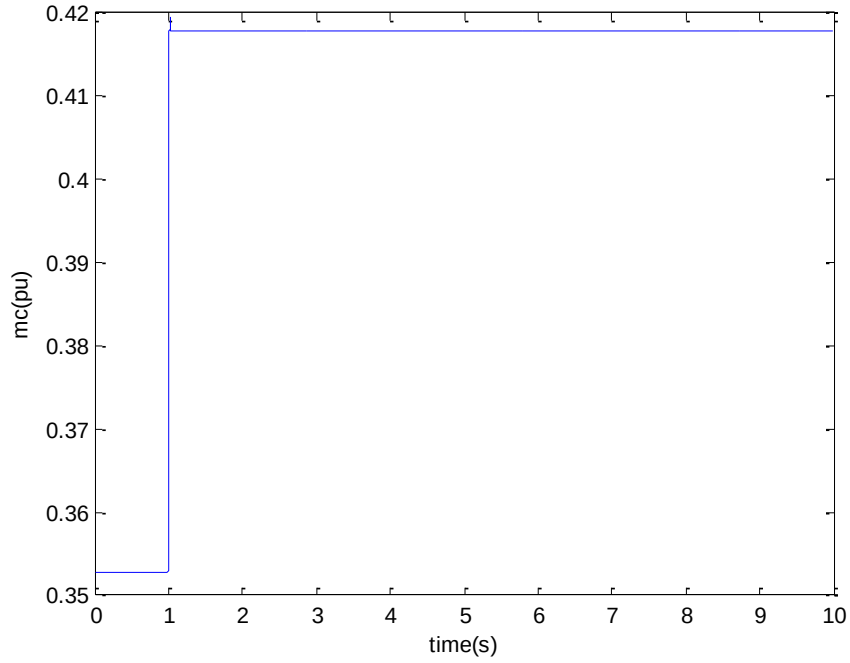

Fig.6.4: compressor output air flow rate

Fig. 6.5 and Fig. 6.6 show the combustion chamber and turbine output mass flow rate, respectively. When load is applied, they increase from 0.356 p.u. to 0.422 p.u.

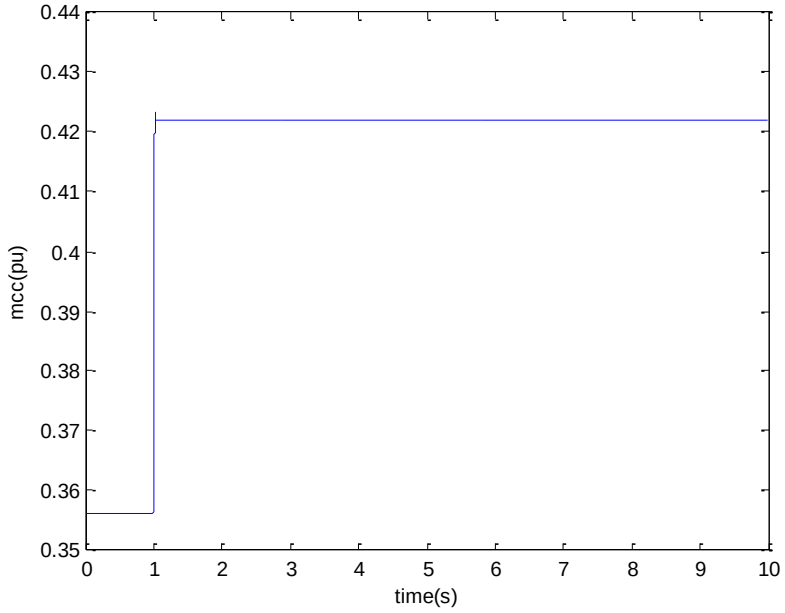

Fig.6.5: combustion chamber output mass flow rate

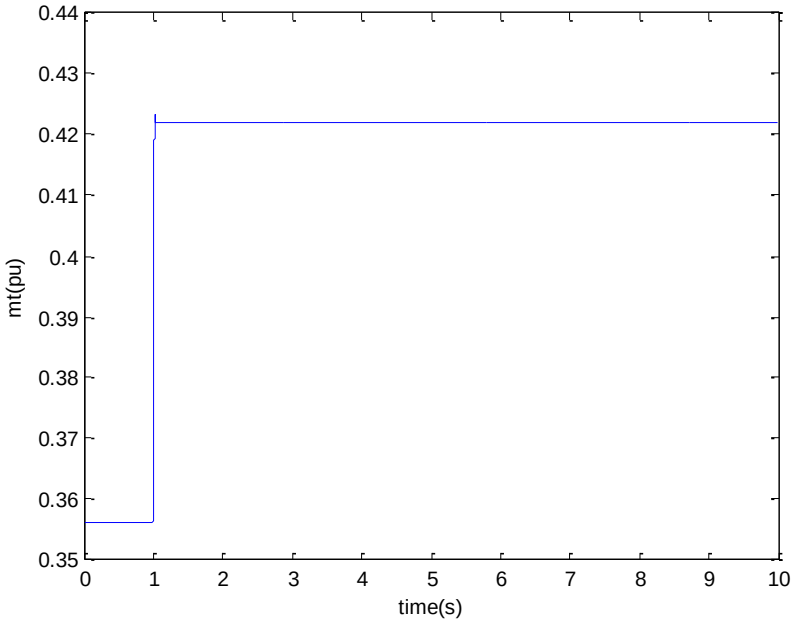

Fig.6.6: turbine output mass flow rate

Fig. 6.7 shows the generated output power of the turbine and Fig. 6.8 shows the mechanical power of the compressor.

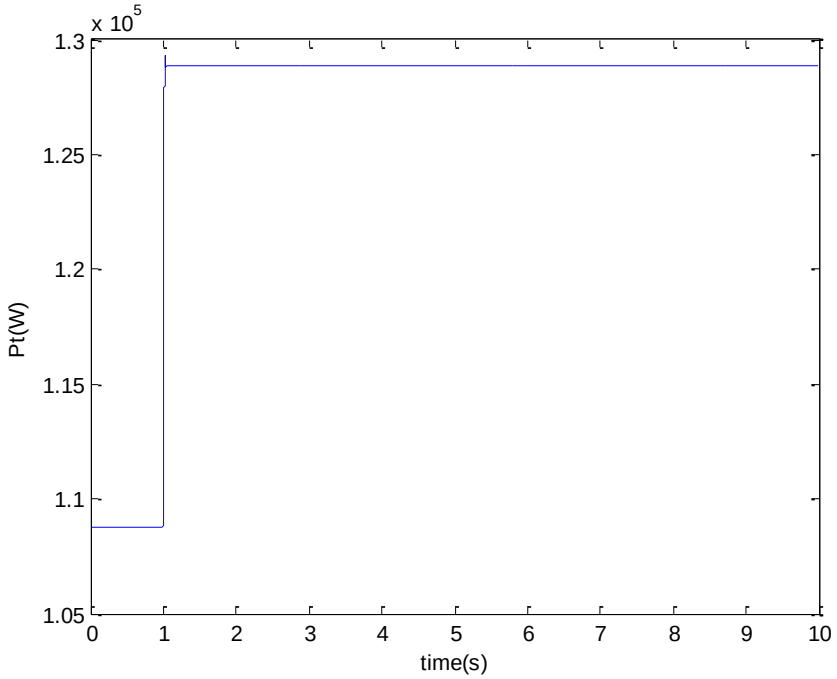

Fig.6.7: turbine output power

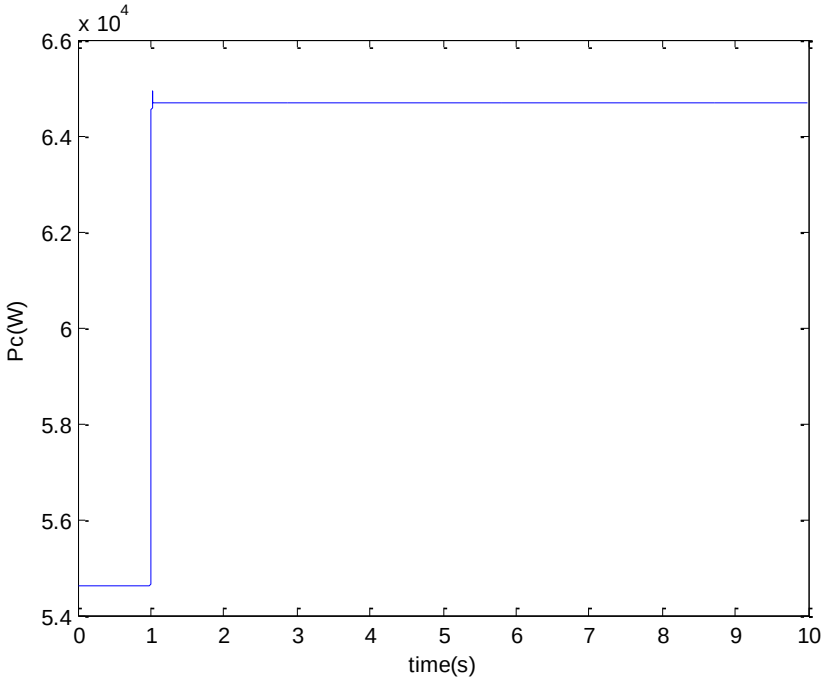

Fig.6.8: mechanical power of the compressor

The variation of stator currents of PMSG are shown in Fig. 6.9 and Fig. 6.10. When load is added, both d and q axis components, after a transient, which is stabilized within a few seconds.

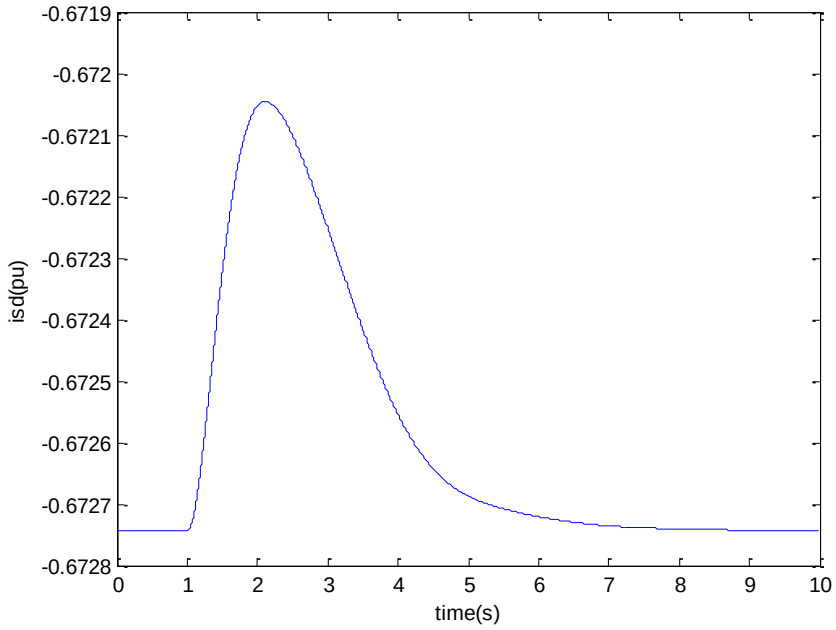

Fig.6.9: *d*-axis component of stator current

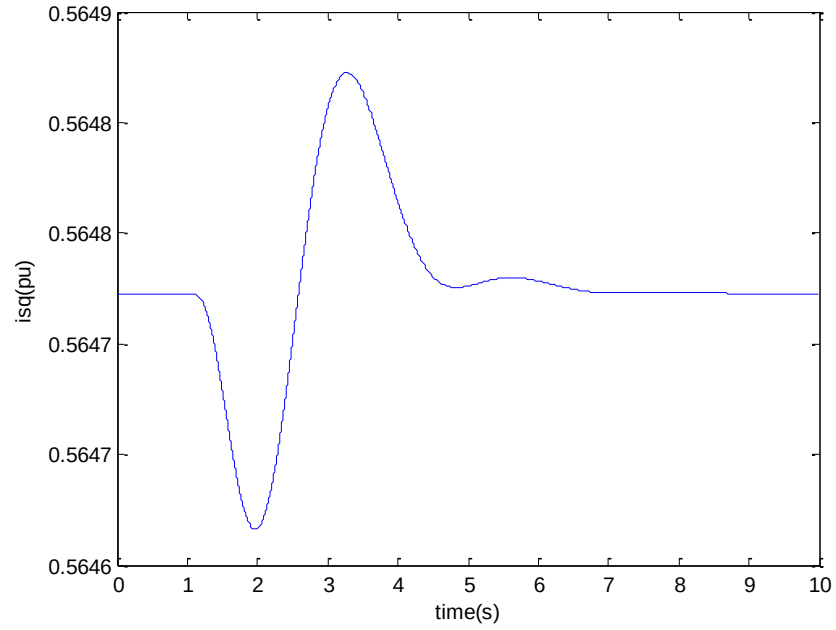

Fig.6.10: *q*-axis component of stator current

Fig. 6.11 shows the change in rotor speed. At no load, rotor speed is 1 p.u. When load is applied, it increases to 1.014 p.u. and takes about 6 seconds to reach the steady state.

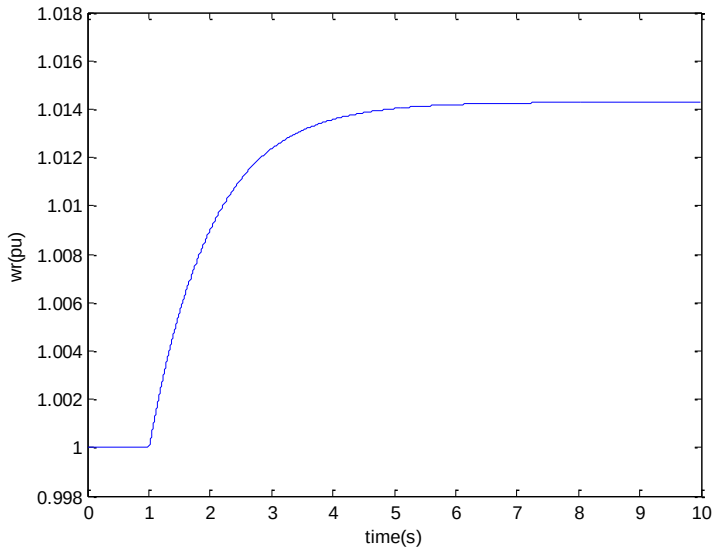

Fig.6.11: rotor speed variation with load

The change in DC link voltage is shown in Fig. 6.12. It exhibits a transient when load is applied and get stabilized within 8 to 9 seconds.

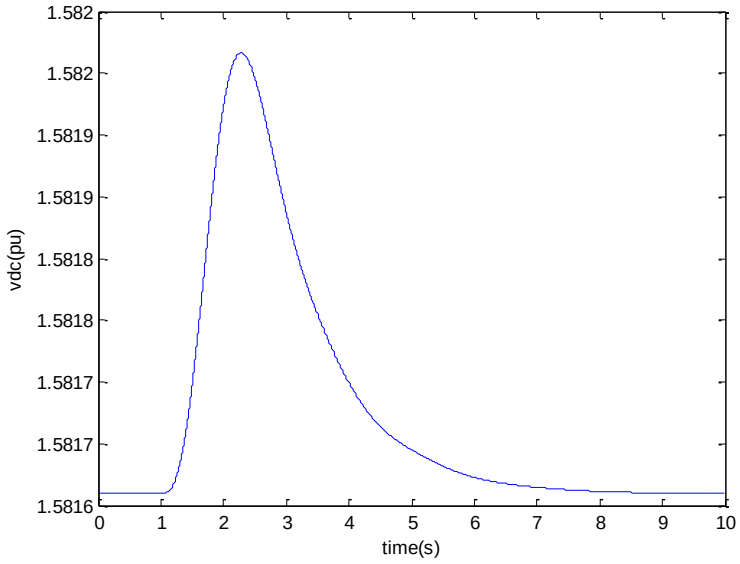

Fig.6.12: DC-link voltage

Fig. 6.13 and Fig. 6.14 show the change in *d* and *q* axis component of grid currents, respectively. When load is applied, d-axis component of grid current increases from 0.5615 p.u. to 0.5680 p.u. but q axis components doesn't change, only shows a transient.

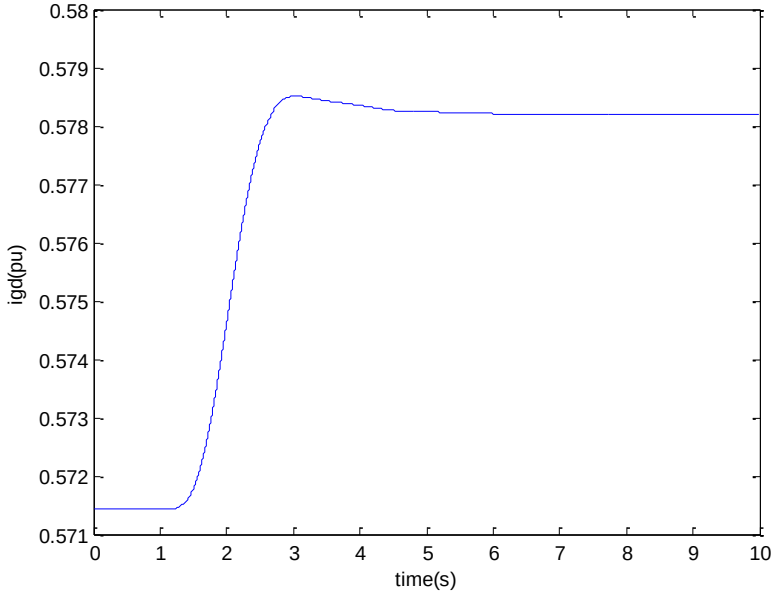

Fig.6.13: *d*-axis component of grid current

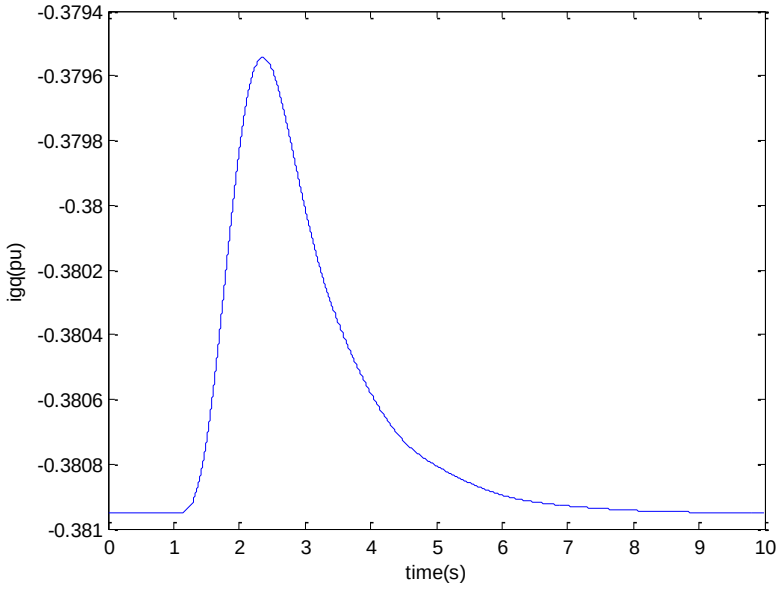

Fig.6.14: *q*-axis component of grid current

Fig. 6.15 exhibits the changes in *d* axis controller parameter of rectifier. On applying load, it decreases and reaches steady state within 6 seconds.

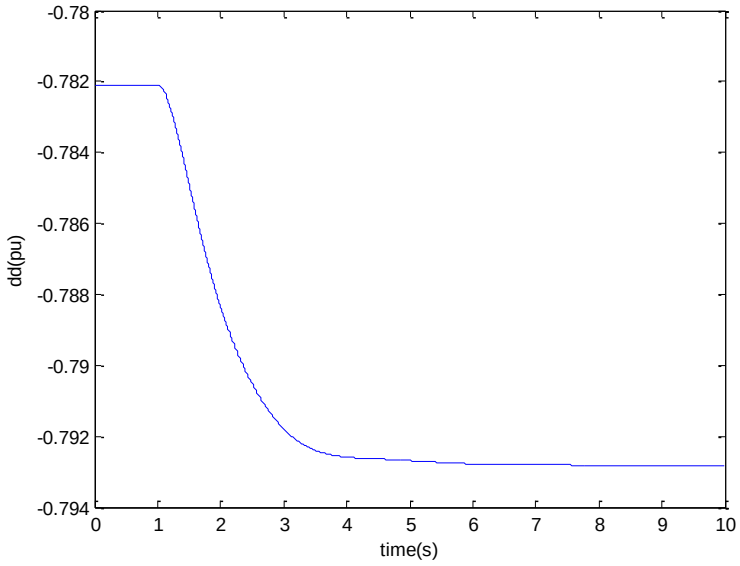

Fig.6.15: *d*-axis component of rectifier switching parameter

The change in *q*-axis controller switching parameter is shown in Fig. 6.16. It decreases and gets stabilized within 6 seconds after load is applied.

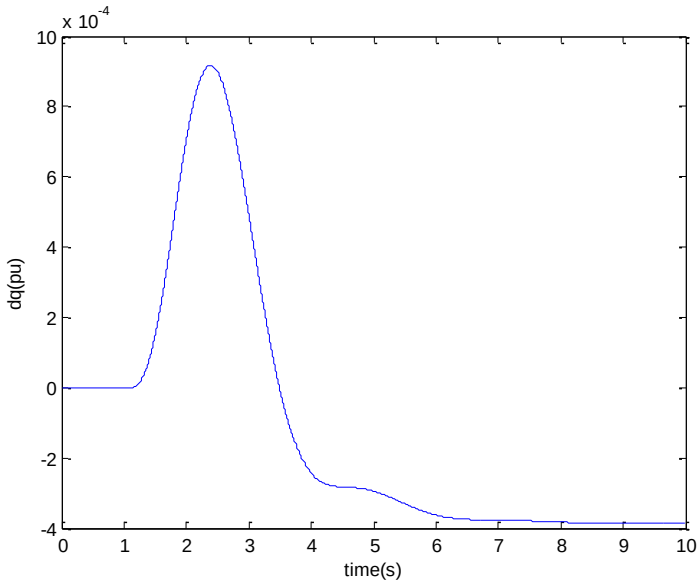

Fig.6.16: *q*-axis component of rectifier switching parameter

Fig. 6.17 and Fig. 6.18, both show the d and q exists switching parameter controller of rectifier and inverter, respectively. They both reach steady state within 5 to 6 seconds.

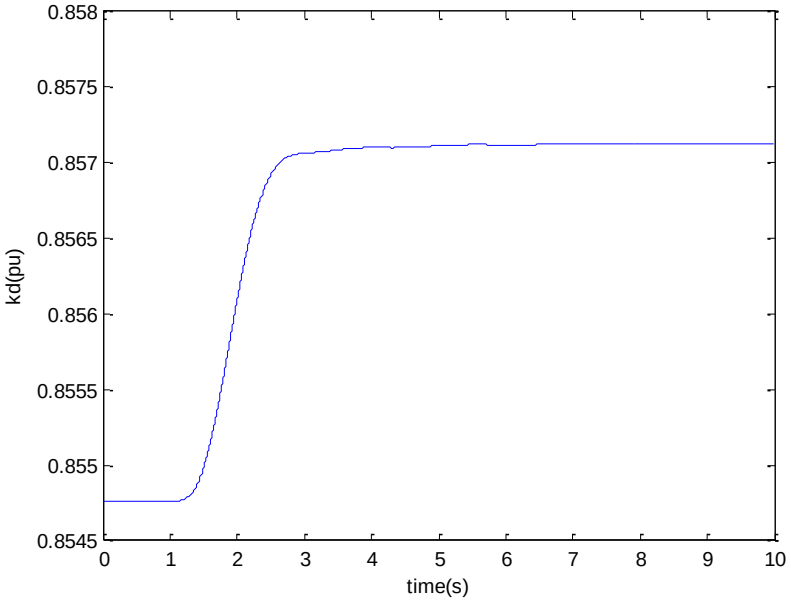

Fig.6.17: *d*-axis component of inverter switching parameter

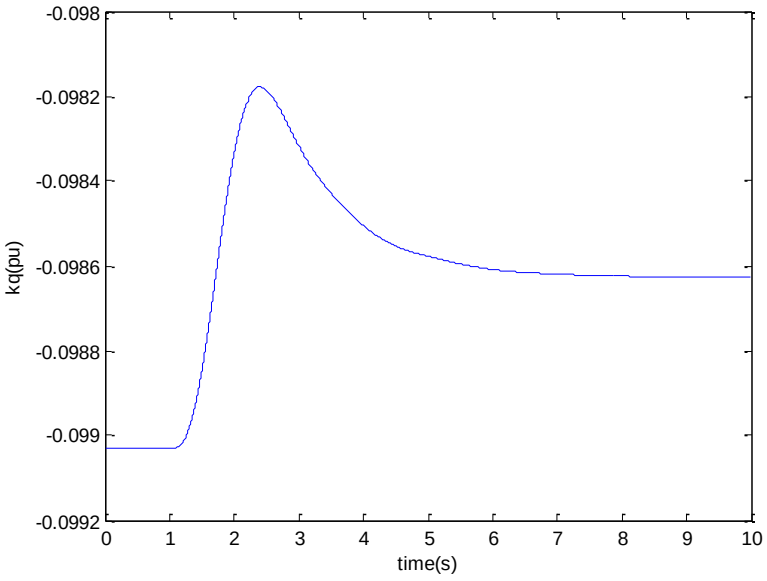

Fig.6.18: *q*-axis component of inverter switching parameter

Chapter 7

Conclusion and Future Work

7.1 Summary and Conclusion

There is a scarcity of models for investigating MTG system as DG particularly for what concerns the integration of power electronics. Dynamic modeling and stability performance of a microturbine coupled with PMSG which is interfaced to utility grid through power conditioning system as a DG, have been presented in this paper. The thesis can be summarized by the following way:

- A thermo-dynamic model of single-shaft, non-recuperated Microturbine have been adopted in this thesis which is suitable for stability analysis in both standalone and grid connected mode.
- The dynamic model of Permanent Magnet Synchronous Generator (PMSG) chosen here is on *dq*-axis reference frame. So the complexity in grid connected analysis is eliminated.

- The switching parameters of the AC-to-DC converter and DC-to-AC inverter is also characterized by *dq*-axis reference frame which is very much essential to connect the PMSG to the grid.
- The above mentioned switching parameters are controlled by PI controllers. The PI controller parameters are selected by a highly efficient optimization tool called the Genetic Algorithm.

7.2 Future Works

- Without delay approximation, real delay can be introduced the Microturbine thermo-dynamic equations.
- The overall stability analysis presented here can be done using Recuperated type Microturbine.
- The overall stability analysis presented here can be done using double-shaft Microturbine.

References

[1] W. I. Rowen, “Simplified mathematical representations of heavy duty gas turbines,” Journal of Engineering for Power, Transactions ASME, vol. 105, no. 4, pp. 865-869, Oct, 1983.

[1] L. N. Hannet and Afzal Khan, “Combustion turbine dynamic model validation from tests,” IEEE Transactions on Power Systems, vol. 8, no. 1, pp. 152-158, Feb. 1993.

[3] Working Group on Prime Mover and Energy Supply Models for System Dynamic Performance Studies, “Dynamic models for combined cycle plants in power system studies,” IEEE Transactions on Power Systems, vol. 9, no. 3, pp. 1698-1708, August 1994.

[4] A. Cano, F. Jurado and J. Carpio, “Influence of micro-turbines on distribution networks stability,” in Proceedings, IEEE PES General Meeting, vol. 4, pp. 2153-2158, Jul. 2003, Toronto, Canada.

[5] F. Jurado and A. Cano, “Use of ARX algorithms for modeling micro-turbines on the distribution feeder,” in Proceedings, IEE: Generation Transmission and Distribution, vol. 151, no. 2, pp. 232-238, Mar. 2004.

[6] Francisco Jurado and Jose Ramon Saenz, “Adaptive control of a fuel cellmicroturbine hybrid power plant,” IEEE Transactions on Energy Conversion, vol. 18 no.2, pp. 342-347, June 2003.

[7] Amer Al-Hinai and Ali Feliachi, “Dynamic model of a microturbine used as a distributed generator,” in Proceedings, 34th Southeastern Symposium on System Theory, Huntsville, pp.209-213, Alabama, March 2002.

[8] H. -J. Nern, H. Kreshman, F. Fischer, and H. A. Nour Eldin, “Modelling of the long term dynamic performance of a gas turbo generator set,” in Proceedings of the Third IEEE Conference on Control Applications, 1994., vol. 1, Aug 1994, pp. 491 – 496.

[9] G. J. Kish, Member, IEEE, and P. W. Lehn, Senior Member, IEEE, "A Micro-turbine Model for System Studies Incorporating Validated Thermodynamic Data"

[10] H. Nikkhajoei and M. R. Iravani, "A matrix converter based microturbine distributed generation system," *IEEE Trans. Power Del.*, vol. 20, no. 3, pp. 2182–2192, Jul. 2005.

[11] Li Wang, Senior Member, IEEE, and Guang-Zhe Zheng, "Analysis of a Microturbine Generator System Connected to a Distribution System through Power-Electronics Converters"

[12] D. N. Gaonkar, and R. N. Patel, "Modeling and Simulation of Microturbine Based Distributed Generation System".

[13] Sanjeev K nayak, D N Gaonkar, "Modeling and Performance Analysis of Microturbine Generation System in Grid Connected/Islanding Operation", INTERNATIONAL JOURNAL of RENEWABLE ENERGY RESEARCH Sanjeev K nayak et al., Vol.2, No.4, 2012.

[14] Larry Goldstein, Bruce Hedman, Dave Knowles, Steven I. Freedman, Richard Woods and Tom Schweizer., "Gas-fired distributed energy resource technology characterizations," National Renewable Energy Laboratory, NREL/TP-620-34783, Nov. 2003.

[15] Y. Zhu and K. Tomsovic, "Development of models for analyzing the load-following performance of microturbines and fuel cells," Journal of Electric Power Systems Research, vol. 62, pp. 1-11, 2002.

[16] D. Yuan, "Energy and exergy evaluations on a microturbine system," Master's thesis, University of Toronto, 2007.

[17] A. Buxbaum, K. Schierau and A. Straughen, Design of Control Systems for DC Drives, ser. EESES Electric Energy Systems and Engineering Series, J.G. Kassakian and D.H. Naunin, Ed. Springer-Verlag, 1990.

[18] D. Yuan, "Energy and exergy evaluations on a microturbine system," Master's thesis, University of Toronto, 2007.

[19] H. Nikkhajoei, "Matrix converter and its application in a micro-turbine based generation system," Ph.D. dissertation, University of Toronto, 2004.

[20] H. -J. Nern, H. Kreshman, F. Fischer, and H. A. Nour Eldin, "Modelling of the long term dynamic performance of a gas turbo generator set," in Proceedings of the Third IEEE Conference on Control Applications, 1994., vol. 1, Aug 1994, pp. 491 – 496.

[21] Web link: http://hyperphysics.phy-astr.gsu.edu/hbase/solids/magperm.html

[22] Mayers

[23] Anders Malmquist, Ola Aglen, Edgar Keller, Marco Suter and Jari Wickstrom., "Microturbines: Speeding the shift to distributed heat and power," ABB Review, no. 3, pp. 22-30, Mar. 2000.

[24] Bimal K.Bose, Modern Power Electronics and AC Drives, Pearson Education, 2003.

[25] Chee-Mun Ong, Dynamic Simulation of Electric Machinery, Prentice Hall, 1998.

[26] Y. Zhu and K. Tomsovic, "Development of models for analyzing the load-following performance of microturbines and fuel cells," Journal of Electric Power Systems Research, vol. 62, pp. 1-11, 2002.

[27] Tatjana Kalitjuka, "Control of Voltage Source Converters for Power System Applications", M.Sc Thesis, Norwegian University of Science and Technology

[28] Md. Apel Mahmud, "Robust Nonlinear Feedback Linearizing Control for Power Systems to Enhance Transient Stability." Master's thesis, The University of New South Wales, 2012.

[29] J. G. Slootweg and W. L. Kling, "Impacts of distributed generation on power system transient stability," in IEEE Power Engineering Society Summer Meeting, vol. 2, 21–25 July 2002, pp. 862–867.

[30] I. Kim, "Robust maximum power point tracker using sliding mode controller for the three-phase grid-connected photovoltaic system," Solar Energy, vol. 81, pp. 405–414, 2007.

[31] S. M. Alizadeh, M. Sedighizadeh and D. Arzaghi-Haris, "Optimization of Micro-Turbine Generation Control System Using Genetic Algorithm", 2010 IEEE International Conference on Power and Energy (PECon2010), Nov 29 - Dec 1, 2010, Kuala Lumpur, Malaysia.

[32] Web link: http://www.mathworks.com

[33] Web link: http://rsif.royalsocietypublishing.org/content/12/103/20141183